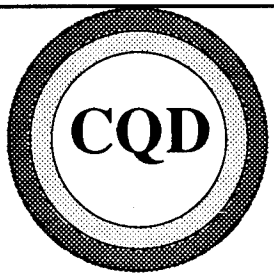

Metalorganic Chemical Vapor Deposition of GaN, AlN and GaAlN for UV Photodetector Applications

Annual Technical Report 7/1/94-3/31/95

Office of Naval Research
Contract #N00014-93-1-0235

Principal Investigator: Manijeh Razeghi

Center for Quantum Devices
Northwestern University
Department of Electrical Engineering
Evanston, IL 60208

Students: Patrick Kung
Adam Saxler
Danielle Walker
Tso-Chun Wang
Xiaolong Zhang

ABSTRACT

GaN, AlN and GaAlN thin films have been grown in a horizontal low-pressure metal-organic chemical vapor deposition. Several types and orientations of substrates have been used, including (00•1), (01•2) and (11•0) sapphire, (00•1) 6H-SiC, (100) and (111) silicon. The starting materials were trimethylgallium, trimethylaluminum and ammonia. The structural, optical and electrical quality of the epilayers has been analyzed through X-ray diffraction, electron microscopy, photoluminescence (PL), optical absorption and Hall effect measurements. Layers with the lowest X-ray rocking curve linewidths ever reported have been achieved on (00•1) sapphire (30 arcsecs for GaN and 100 arcsecs for AlN). Transmission electron microscopy for the GaN films showed the high crystalline quality of the layers as well as that of the interfaces. Photoluminescence at 300 K and 77 K yielded typical linewidths of about 80 meV and 40 meV respectively, on (00•1) sapphire. Although the crystalline quality of the epilayers on silicon was not as good as on basal plane sapphire, the photoluminescence results were comparable to those on (00•1) sapphire in terms of linewidths. The crystalline quality of the films on 6H-SiC was not as good as expected because of the lower quality of the SiC substrates used. However, no deep-level associated luminescence could be detected from the GaN on SiC. The optical absorption of films on sapphire revealed sharp cut-offs at the band edge for GaN and AlN films. Unintentionally n-type doped GaN layers yielded an electron mobility as high as 200 cm^2/Vs. More recently, as-grown semi-insulating GaN films have been achieved. The n-type doping control of GaN has been realized by incorporating Ge. Electron concentrations of up to 10^{20} cm^{-3} were obtained. The p-type doping of GaN has been carried out by incorporating Mg, and the as-doped layers were semi-insulating. Unlike undoped GaN, the deep-level associated yellow luminescence emission could not be detected from doped films. This suggests the origin of the yellow emission may be due to Ga vacancies, since Ge and Mg occupy Ga sites. The temperature variation of the PL spectra for doped samples yielded the thermal activation energies associated to the dopant levels. Ternary $Ga_{1-x}Al_xN$ compounds have been grown through the entire compositional range ($0 \leq x \leq 1$). Optical absorption showed a good tailoring of the bandgap with composition, while keeping sharp cut-offs. Elementary photoconductors have been realized with GaN and $Ga_{1-x}Al_xN$ layers, using the Van der Pauw geometry. The lifetimes of excess carriers have been investigated, which would allow to predict the performance of photoconductive devices realized with these materials. The processing of GaN and GaAlN films, including the deposition and annealing of contacts, the realization of interdigitated contacts, has been realized.

TABLE OF CONTENTS

I. INTRODUCTION

UV Photodetectors

There exist numerous applications for ultraviolet (UV) photodetectors, including the surveillance and recognition of spacecraft, space-to-space communications, the monitoring of welding as well as engines and combustion chambers. The main characteristics of these devices should present are a solar blindness (to distinguish a spacecraft from a decoy), a high sensitivity, a high speed response, a robustness to extreme conditions (heat and/or radiations).

The detection of light in the UV spectral region can be achieved by using photocathodes or solid-state detectors such as charge-coupled devices (CCDs). Compared to photocathodes, solid-state detectors present advantages that have already been demonstrated by conventional Si CCDs: high spatial resolution, robustness, light weight, large dynamic range, and low readout noise. Although Si is still the material of choice for these devices, future detectors are expected to offer the following characteristics: solar blindness, high quantum efficiency in the UV, and low dark current/low noise. To date, the UV detector technology mainly involves Si, and more recently SiC wide bandgap SiC which offers a better solar blindness, lower noise, and is a more robust material than Si.

However, the aerospace, automotive, petroleum and other industries continuously provide the impetus for the development of new material technologies that would be tolerant to increasing temperatures and hostile environments. Consequently, the most promising material system for future UV photodetectors is GaAlN compounds (later called III-Nitrides). A bandgap energy range from 3.4 eV (365 nm, GaN) to 6.2 eV (200 nm, AlN) can be covered, thus allowing a good tailoring of the cut-off wavelength by varying the alloy composition. The direct bandgap of GaAlN results in a higher absorption coefficient, a sharper cut-off and a higher response speed than SiC. Another advantage of GaAlN is the possibility to realize heterojunctions within this material system, thus improving then quantum efficiency. Finally, GaAlN are extremely stable to physical and chemically harsh environments.

Research work conducted at the CQD

The objective of this project is to investigate the growth of high quality GaN, AlN and GaAlN compounds in order to realize UV photodetectors.

The Center for Quantum Devices (CQD) started the growth and characterization of III-Nitrides by using an atmospheric pressure metalorganic chemical vapor deposition

(MOCVD) reactor. In a short time, state-of-the-art results have been achieved.[1-7] However, the limited capability of that reactor has been reached early in 1994:

- The use of more than two organometallic (OM) sources would have required their mixing with the hydride source before the reaction chamber. This prevented the use of any OM p-type doping source.
- The elementary gas handling system prevented the use of any hydride n-type doping sources.
- The operation at atmospheric pressure limited the uniformity and homogeneity of the films, which is detrimental to the realization of large area photodetectors.

In view of these limitations, the CQD has acquired and is developing a low pressure MOCVD reactor, built by AIXTRON GmbH. This system will be described in section II. Within a short period of time, the whole III-Nitride activity has been successfully transferred to this new MOCVD reactor. The expected improvements of the material quality were obtained and world class results for GaN, AlN, GaAlN, n-type doping of GaN, and photoconductivity using these materials have been achieved. These will be described in this report.

References

1- "*Thermal stability of GaN thin films grown on (00•1) Al_2O_3 , (01•2) Al_2O_3 and (00•1)$_{Si}$ 6H-SiC substrates*"
C.J. Sun, P. Kung, A. Saxler, H. Ohsato, E. Bigan, and M. Razeghi; D.K. Gaskill, Journal of Applied Physics 76(1), 236 (1994).

2- "*Crystallography of epitaxial growth of wurtzite-type thin films on sapphire substrates*"
P. Kung, C.J. Sun, A. Saxler, H. Ohsato, and M. Razeghi,
Journal of Applied Physics 75(9), 4515 (1994).

3- "*A crystallographic model of (00•1) aluminum nitride epitaxial film grown on (00•1) sapphire substrate*"
C.J. Sun, P. Kung, A. Saxler, H. Ohsato, K. Haritos, and M. Razeghi,
Journal of Applied Physics 75(8), 3964 (1994).

4- "*High quality aluminum nitride epitaxial layers grown on sapphire substrates*"
A. Saxler, P. Kung, C.J. Sun, E. Bigan, and M. Razeghi,
Applied Physics Letters 64(3), 339 (1994).

5- "*$Al_xGa_{1-x}N$ grown on (00•1) and (01•2) sapphire*"
C.J. Sun, P. Kung, A. Saxler, H. Ohsato, and M. Razeghi,

Inst. Phys. Conf. Ser. No 137, Chapter 4, 425-428, proceedings of the 5th International Conference on Silicon Carbide and Related Materials, Washington, DC, Nov. 1-3, 1993.

6- "*Comparison of the physical properties of GaN thin films deposited on (00•1) and (01•2) sapphire substrates*"
C.J. Sun and M. Razeghi,
Applied Physics Letters 63(7), 973 (1993).

7- "*Improvements on the structural and electrical properties of GaN thin films grown by metalorganic chemical vapor deposition using different substrate orientations*"
C.J. Sun and M. Razeghi,
Accepted for poster presentation, to be published in the proceedings of SPIE, March 5, 1993.

II. EXPERIMENTAL PROCEDURES

NEW Low-Pressure MOCVD reactor

The new low pressure MOCVD system that the CQD acquired has been specifically designed to overcome the limitations of the old system:

- It allows the use of 6 OMs, including principally trimethyl-gallium (TMGa), trimethyl-aluminum (TMAl), bis-cyclopentadienyl-magnesium (Cp_2Mg), diethyl-zinc (DEZn). Seven hydride sources are also connected, including principally ammonia (NH_3), germane (GeH_4), silane (SiH_4) and hydrogen chloride (HCl) for cleaning purposes. The sources have been carefully chosen for their high purity. A hydrogen purifier allowed to use extremely pure hydrogen (H_2) as carrier gas and preserve the purity of the OMs.
- The purity of the growth chamber is kept by systematic cleaning procedures before and after each growth. A glove box filled with filtered nitrogen is used for the loading and unloading of the samples, as well as isolate the reaction chamber from the atmosphere.
- A low growth pressure, down to 10 mbar (7.6 Torr), associated with a rotating graphite susceptor disk (rotation speed up to about 100 rpm), allows the growth of highly uniform and homogeneous films. This property is most important for large area photodetectors.

This reactor is the first of its kind to grow III-Nitrides and the CQD is constantly improving its design in order to further optimize the quality of III-Nitride materials. As a consequence, some technical modifications are often needed for necessary improvements.

Growth parameters

The epitaxial growths have been performed on different types and orientations of substrates, including (00•1), (01•2) and (11•0) sapphire (Al_2O_3), (00•1) 6H-SiC, (100) and (111) Si. The use of sapphire and SiC substrates is clear because of their hexagonal symmetry which is similar to that of III-Nitrides. The motivation in using silicon substrates resides in the potential to realize integrate III-Nitride based UV photodetectors with the well established Si circuit electronics. The degreasing of the substrates was done through a few minutes in hot trichloroethylene, acetone, hot methanol, propanol solutions (in this order). Then, the sapphire substrates were etched in a hot H_2SO_4:H_3PO_4=3:1 acidic solution for several minutes, while the SiC and Si substrates were etched by dipping into hydrofluoric acid. These cleaning steps proved good enough in order to obtain the results presented here.

Several growth parameters have been optimized, including V/III molar ratio, growth temperature, growth pressure, growth rate, buffer layer type and thickness. These can be summarized in Table II-A. Confirming its previous experience, the CQD has proved that a high temperature AlN buffer layer improves the quality of the GaN bulk film, while no buffer is needed in order to obtain high quality AlN (Section III). Bulk epilayers are usually about 1 to 2 μm thick, which is sufficient for characterization and optimization purposes.

Growth parameter	Range of operation	Optimum for GaN	Optimum for AlN
V/III molar ration	200 - 3000	1000 - 2000	~ 2500
Growth temp.	850 - 1000 °C	~ 1000 °C (10 mbar)	~ 1000 °C
Growth pressure	10 or 100 mbar	no significant difference (except growth T)	no significant difference
Growth rate	0.25 - 1.5 μm/hr (GaN) 0.15 to 1 μm/hr (AlN)	~ 0.7 μm/hr	~ 0.15 μm/hr
Buffer layer	AlN, GaN or none	~350 Å AlN (same growth conditions as bulk AlN)	none

Table II-A. Range of operation of the growth parameters

In general, in spite of its big lattice and thermal mismatch with III-Nitrides, basal plane sapphire is still the most suited substrate to obtain the best structural, optical and electrical properties of GaN and AlN. Materials grown on (00•1) 6H-SiC did not yield as good properties because of the much lower quality of the SiC wafers available at the CQD. Finally, high quality single-crystal III-Nitride layers have been obtained on Si substrates.

After each growth, the reactor is cleaned with HCl. The quartz ware is usually cleaned by using an aqua regia solution, followed by a thorough rinsing with de-ionized water and an oven bake before re-insertion in the growth chamber. These cleaning steps

have proved most useful, because the growth of III-Nitrides leaves a significant amount of deposition in the reactor chamber.

Characterization techniques

In order to provide feedback to the epitaxial growth, as well as get insight into the physical properties of III-Nitride materials, several characterization techniques are systematically used.

An optical microscope is used to probe the film surface morphology. The thickness of the films is determined by a ball polishing technique, and is usually confirmed by optical absorption. X-ray diffraction, using a five-crystal diffractometer, and (scanning, transmission) electron microscopy are used to assess the macro- and micro-structural quality of the films. The optical quality is first determined through photoluminescence (PL) from 300 K down to 77 K, using a He-Cd laser (325 nm, ~10 mW) and a standard PL emission collection setup. Because of the laser wavelength, only $Ga_{1-x}Al_xN$ films with $x \leq 0.15$ can be characterized through PL. Photoluminescence also allows the characterization of doping levels in the bandgap. Optical absorption at 300 K, and Fourier transform infrared spectroscopy are used to determine the optical properties of the layers. Hall effect measurements allow the determination of the carrier concentrations and mobilities in the layers.

III. UNDOPED BINARY COMPOUNDS GaN AND AlN

Introduction

GaN and AlN are the two endpoints of the $Ga_{1-x}Al_xN$ alloy system. GaN has been the most widely studied III-Nitride material, while AlN and GaAlN ternary compounds have received less attention.[1] This is because the research work on III-Nitride materials is currently driven by the quest towards blue emitters, for which GaN are best suited.[2] Another reason is because it is more difficult to achieve high quality materials and control the electrical properties when incorporating Al into GaN. However, because of the numerous applications of photodetectors operating in the UV, a tailored cut-off wavelength between 200 and 365 nm is preferred. Consequently, high quality GaAlN materials must be achieved for a complete composition range. The first task is to optimize the growth of AlN and GaN.

Aluminum nitride

Following its previous experience with the old atmospheric MOCVD system, the CQD started with optimization of AlN thin films, since they will be used as buffer layers in the optimization of GaN bulk layers. The range for growth parameters and the optimum growth conditions are given in Table II-A. This optimization has been realized within the first few growths.

Structural characterization on (00•1)Al_2O_3

High quality AlN thin films have been achieved on basal plane sapphire. The layers were about 0.3 μm thick as determined by ball polishing, they were transparent, while the surface morphology was smooth and featureless. An X-ray rocking curve (XRC) linewidth of about 100 arcsecs has been achieved (Fig. III-1 (bottom)) [3], which is similar to the high quality AlN reported earlier using the old atmospheric pressure MOCVD reactor.[4] However, the observed Pendellösung oscillations in the X-ray diffraction spectrum demonstrate a higher quality of the AlN films and interfaces compared to the films grown with the old system. To the best of our knowledge, such oscillations for AlN have never been reported by other groups. The layer thicknesses have been confirmed by measuring the spacing between these oscillations.[5]

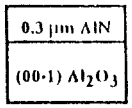

Best Aluminum Nitride / Sapphire

Optical transmission:

- A sharp cut-off at the absorption edge at 6.1 eV can be seen.
- The Fabry-Perot interference fringes confirm the measured thickness.

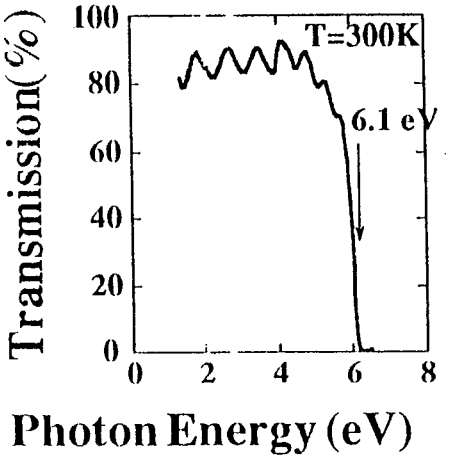

X-ray rocking curve:

- Pendellösung oscillations are observed for AlN for the first time in the world.
- The Pendellösung oscillations confirm the high quality of the epilayers.
- They also confirm the measured thickness.

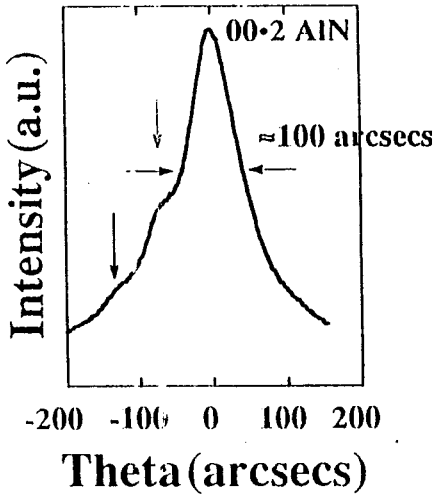

Conclusion: We obtained the best AlN epilayers ever reported.

FIGURE III-1

Gallium Nitride on Silicon

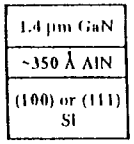

X-ray diffraction of GaN / (111)Si

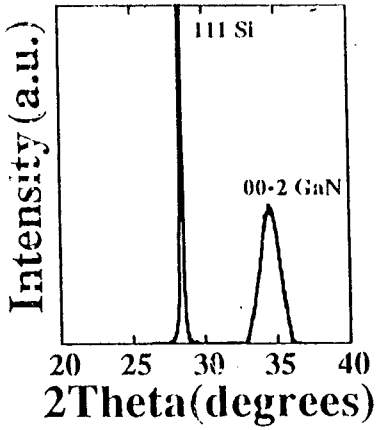

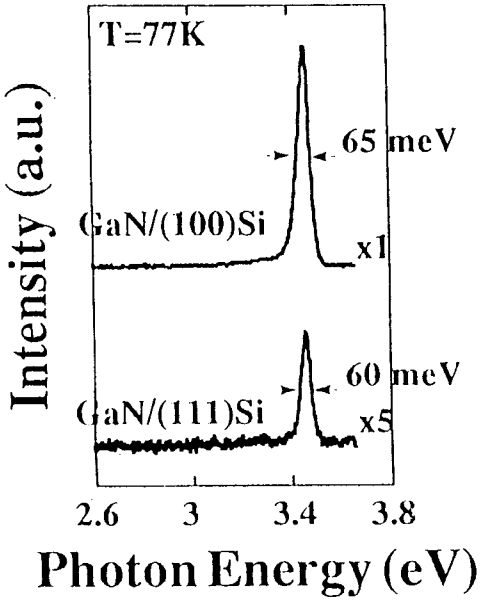

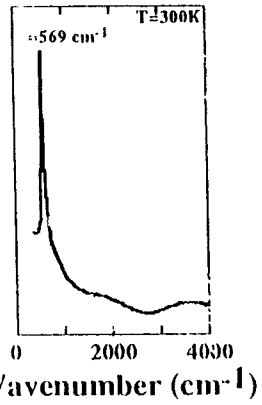

Photoluminescence:

- Sharp donor bound excitonic emission at 3.46 eV.

Infrared absorption:

- Sharp phonon absorption peak at ~569 cm^{-1}.

Conclusion: Single crystal, optically active GaN grown on silicon substrates.

Aluminum Nitride on Silicon

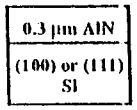

X-ray diffraction of AlN / (111)Si

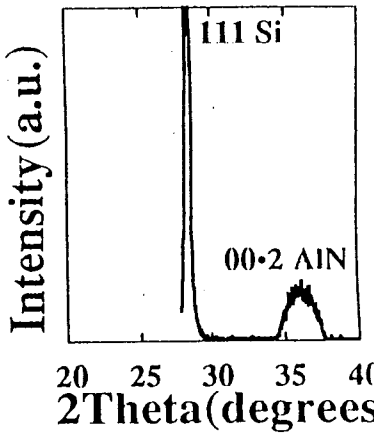

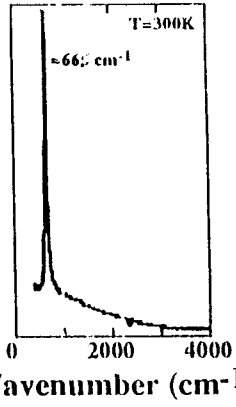

Infrared absorption:

- Sharp phonon absorption peak at ~665 cm^{-1}.

Conclusion: Single crystal AlN grown on silicon substrates.

FIGURE III-2

Optical and electrical characterization on (00•1)Al_2O_3

The optical transmission in the UV-visible spectral region has been measured at 300 K for AlN grown on (00•1)Al_2O_3 (Fig. III-1 (top)). By fitting the square of the absorption coefficient near the absorption edge, a very sharp absorption edge at 6.1 eV can be determined. Fabry-Perot oscillations confirm the high quality and uniformity of the interfaces and the films. By using the refractive indices of AlN [6], the layer thicknesses were calculated and were in good agreement with other thickness measurements.

All AlN epilayers were highly resistive, preventing any electrical measurement.

Aluminum nitride on Si

Single crystal AlN layers have been successfully obtained on Si substrates (Fig. III-2 (top right)) using the same growth conditions as for the growth on basal plane sapphire. The AlN diffraction peak full width at half maximum (FWHM) was about 80 arcmins. The structural quality was further assessed through FTIR at 300K which revealed a sharp phonon absorption peak at 665 cm^{-1}, corresponding to the TO phonon mode of AlN (Fig. III-2 (bottom right)).

Gallium nitride

Immediately after achieving high quality AlN layers, the growth of GaN has been optimized. Following its previous experience, the CQD has used AlN buffer layers grown in the same conditions as for bulk AlN growth. The range for growth parameters and the optimum growth conditions are given in Table II-A. After thorough optimization, world-class single crystal GaN films have been achieved at the CQD.

Structural characterization on (00•1)Al_2O_3

The epilayers were about 1.4 μm thick, as determined by ball polishing. The films were transparent with a featureless surface morphology. An X-ray rocking curve FWHM of about 30 arcsecs (00•2 diffraction peak of GaN) has been obtained for films on basal plane Al_2O_3 (Fig. III-3 (left)), which is among the lowest value ever reported in the literature.[7,8] This represent a major achievement since the narrowest linewidth obtained with the old MOCVD system was about 10 times larger than the linewidth obtained with the new MOCVD system. A simple theoretical calculation allowed to estimate the narrowest XRC linewidth that can be achieved for the 00•2 diffraction peak of GaN, when the GaN is perfectly single crystal, infinitely thick and the diffraction spectrum is measured with an ideal diffractometer. A value of 33.2 arcsecs was obtained [3], which is similar to the

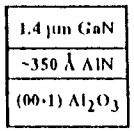

Best Gallium Nitride / Sapphire

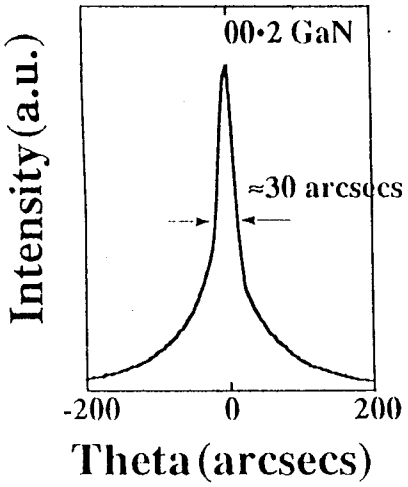

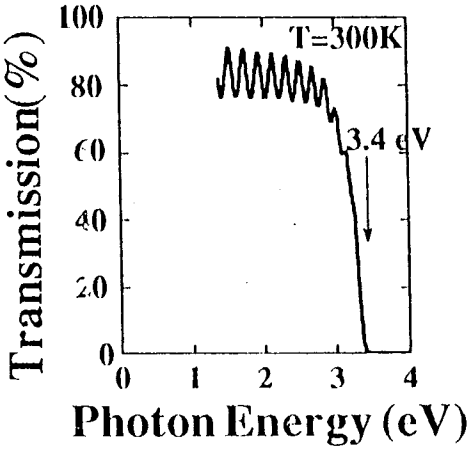

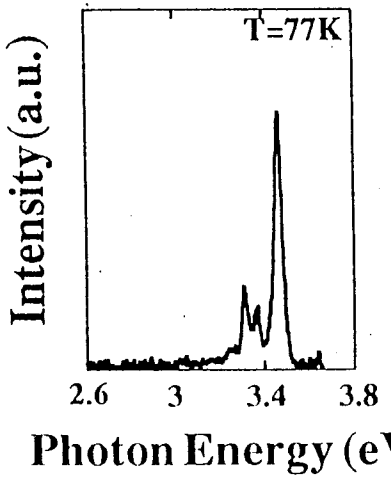

X-ray rocking curve:

- 30 arcsecs: narrowest linewidth ever reported.

Optical transmission:

- Sharp cut-off at the absorption edge at 3.4 eV.
- Fabry-Perot interference fringes can also be seen.

Photoluminescence:

- Sharp donor bound excitonic emission at 3.46 eV. (FWHM~4 meV at 4 K).
- The other two peaks are phonon replicas and shallowimpurityrelated emissions.

Electrical data:

- μ(300K) ≈ 200 cm^2/Vs and n(300K) ≈ 10^{18} cm^{-3}
- or as-grown semi-insulating layers

Conclusion: We obtained the best GaN single crystal ever reported

GaN/AlN-TEM#2

Center for Quantum Devices

CQD

GaN/AlN on Sapphire

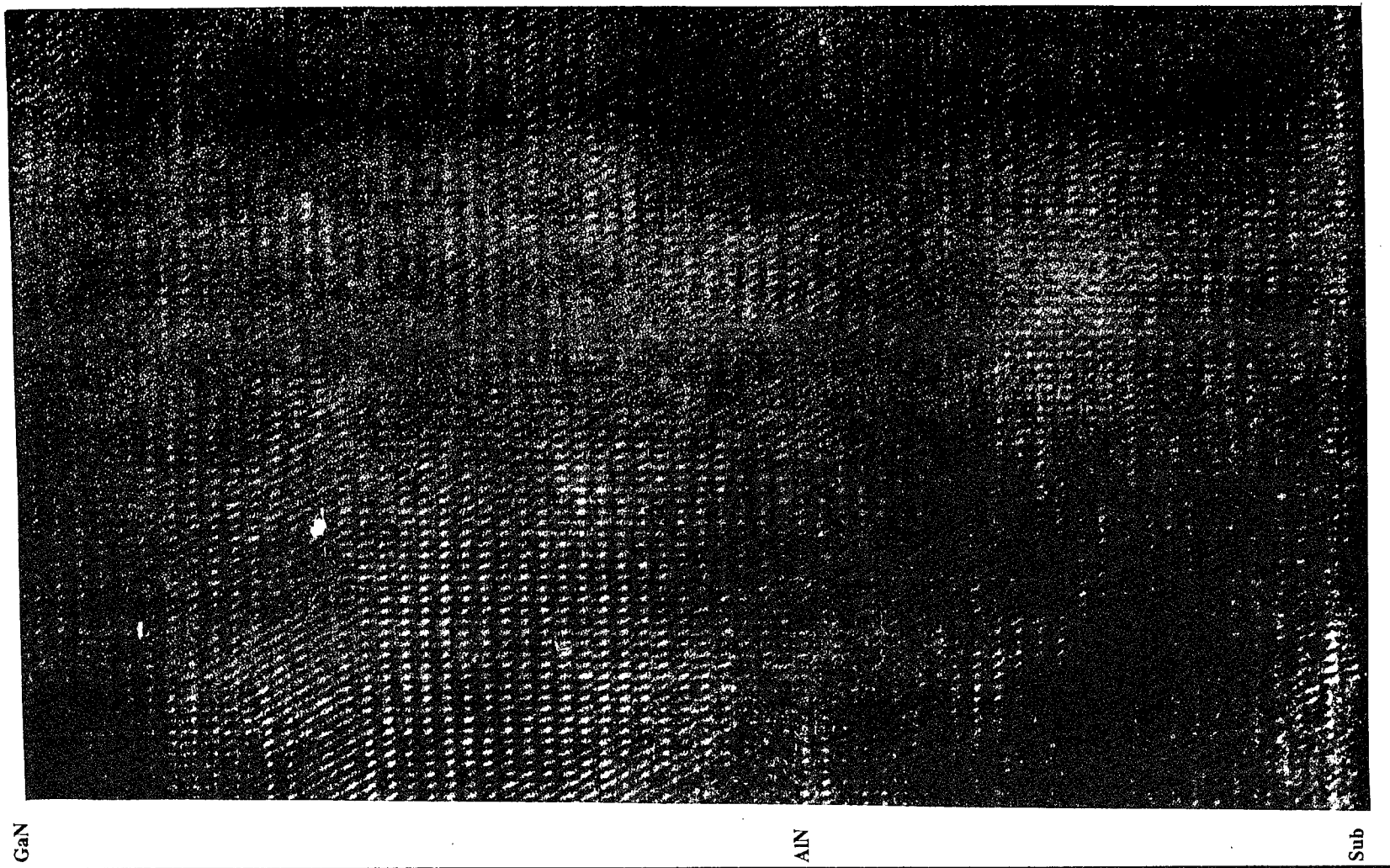

FIGURE III-4

Northwestern University

value obtained here and suggests that the highest degree of crystal perfection has been realized in these GaN layers.

To further investigate the structural quality, high resolution transmission electron microscopy (TEM) has been performed (Fig. III-4). The microstructural quality of the AlN buffer layer and the GaN layer, as well as the quality of the GaN/AlN and AlN/Sapphire interfaces are clear on such micrographs.

Optical characterization on (00•1)Al_2O_3

The optical transmission at 300 K has been measured for GaN grown on (00•1)Al_2O_3 (Fig. III-3 (middle)). A very sharp absorption edge at 3.4 eV can be determined by fitting the square of the absorption coefficient near the absorption edge. Once again, the Fabry-Perot oscillations confirm the high quality and uniformity of the interfaces and the films. By using the refractive indices of GaN [9], the film thicknesses were estimated and confirmed the ball polishing measurements.

The optical properties of the epilayers have also been characterized through photoluminescence at 300 K and 77 K. At 300 K, near band edge emission could be detected at 3.4 eV, as well as the deep-level associated yellow emission at about 2.2 eV. At 77 K, a sharp donor-bound excitonic emission could be clearly seen at 3.46 eV, with a linewidth of about 40 meV (Fig. III-3 (right)). More interestingly, two additional emissions at 3.41 and 3.37 eV have also been observed at 77 K. Phonon replicas of the excitonic line, with a phonon energy of about 40-50 meV, may explain the presence of such peaks because of the high crystalline quality of the GaN epilayer. However, the emission line at lower energy (3.37 eV) is more intense than the one at higher energy (3.41 eV), which suggests that an additional effect contributes to such spectrum. There have been few reports concerning these two emission lines.[10,11] The two interpretations, involving 'hydrogen-induced' donor states and band-to-shallow acceptor transitions are both consistent with the spectrum shown here.

Gallium nitride on other orientations and types of substrate

Using the AlN buffer layer technique described previously, the GaN epilayers grown on other orientations of Al_2O_3 substrates generally yielded wider X-ray diffraction peaks (Fig. III-5): the linewidths were about 20 and 40 times larger for GaN on (11•0) and (01•2)Al_2O_3 respectively, than on (00•1)Al_2O_3. The near band edge luminescence emissions at 300 K and 77 K also had wider linewidths (Fig. III-6a and III-6b): they were about twice as large as on basal plane sapphire for GaN layers on (01•2)Al_2O_3. These

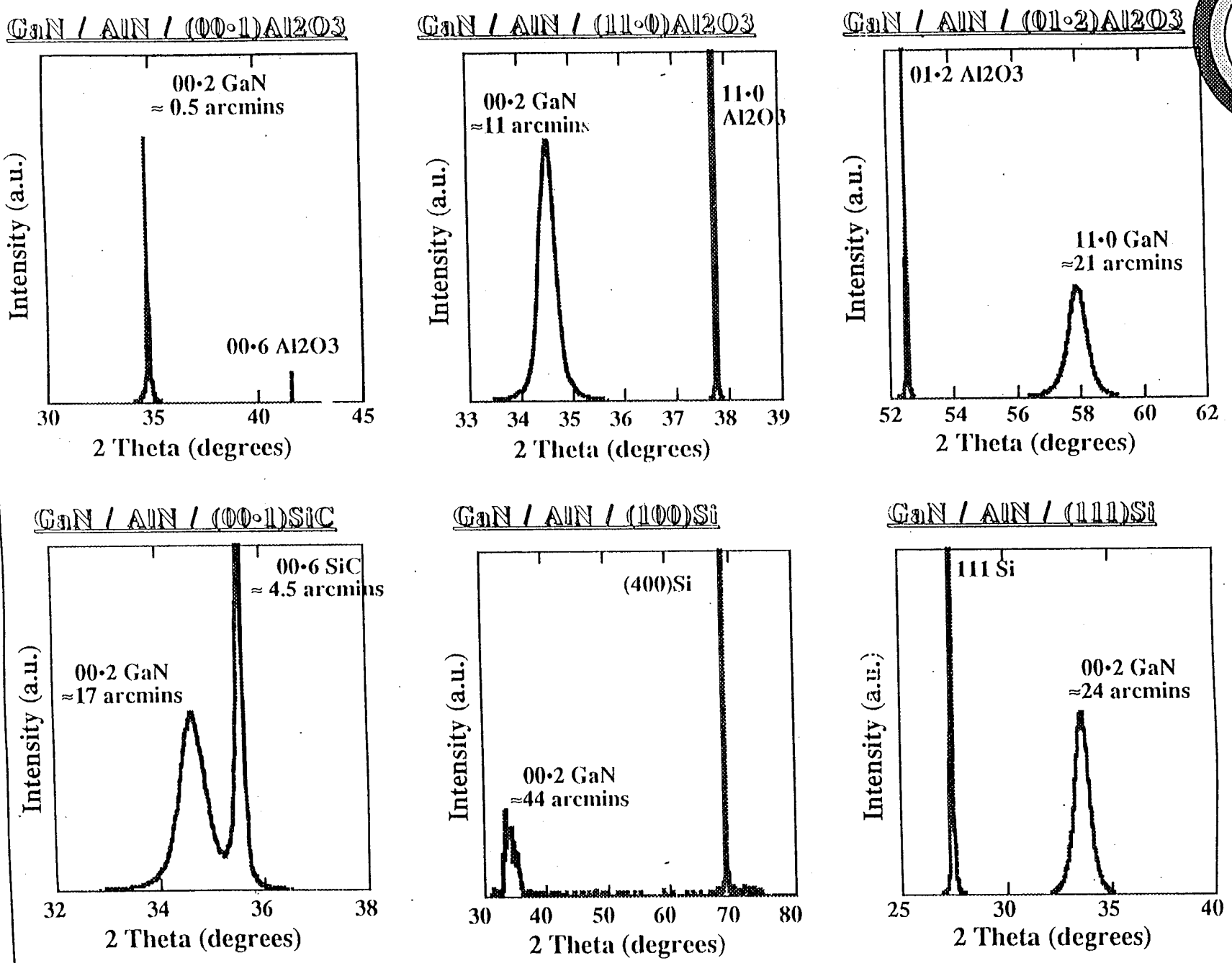
GaN / AlN / (00•1)Al2O3
00•2 GaN
≈ 0.5 arcmins
00•6 Al2O3
Intensity (a.u.)
30 35 40 45
2 Theta (degrees)
GaN / AlN / (11•0)Al2O3
00•2 GaN
≈11 arcmins
11•0
Al2O3
Intensity (a.u.)
33 34 35 36 37 38 39
2 Theta (degrees)
GaN / AlN / (01•2)Al2O3
01•2 Al2O3
11•0 GaN
≈21 arcmins
Intensity (a.u.)
52 54 56 58 60 62
2 Theta (degrees)
GaN / AlN / (00•1)SiC
00•6 SiC
≈ 4.5 arcmins
00•2 GaN
≈17 arcmins
Intensity (a.u.)
32 34 36 38
2 Theta (degrees)
GaN / AlN / (100)Si
(400)Si
00•2 GaN
≈44 arcmins
Intensity (a.u.)
30 40 50 60 70 80
2 Theta (degrees)
GaN / AlN / (111)Si
111 Si
00•2 GaN
≈24 arcmins
Intensity (a.u.)
25 30 35 40
2 Theta (degrees)

FIGURE III-5

Room Temperature Photoluminescence of GaN on Different Substrates

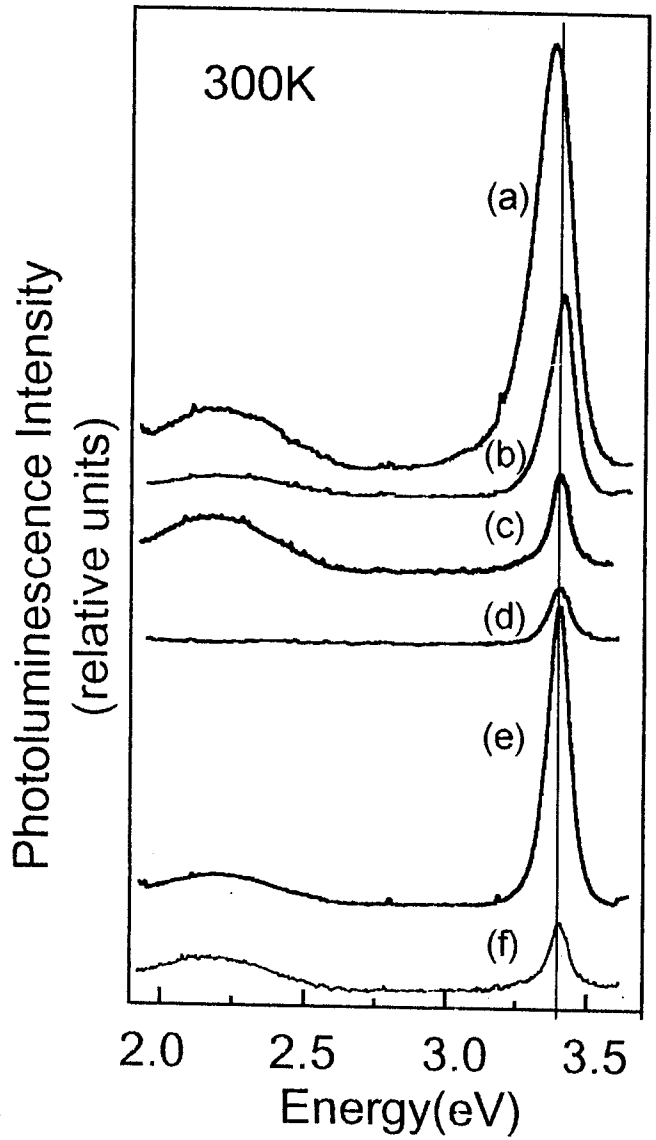

From Top to bottom

Substrate	Eg(eV)	FWHM(meV)
(a) Al_2O_3 (01.2)	3.372	159.5
(b) Al_2O_3 (11.0)	3.407	106.1
(c) Al_2O_3 (00.1)	3.402	82.2
(d) 6H-SiC	3.400	98.7
(e) Si(100)	3.400	93.7
(f) Si(111)	3.402	87.5

Conclusion:

Realization of efficient room temperature photoluminescence of GaN on different substrate orientations

FIGURE III-6a

77K Photoluminescence of GaN on Different Substrates

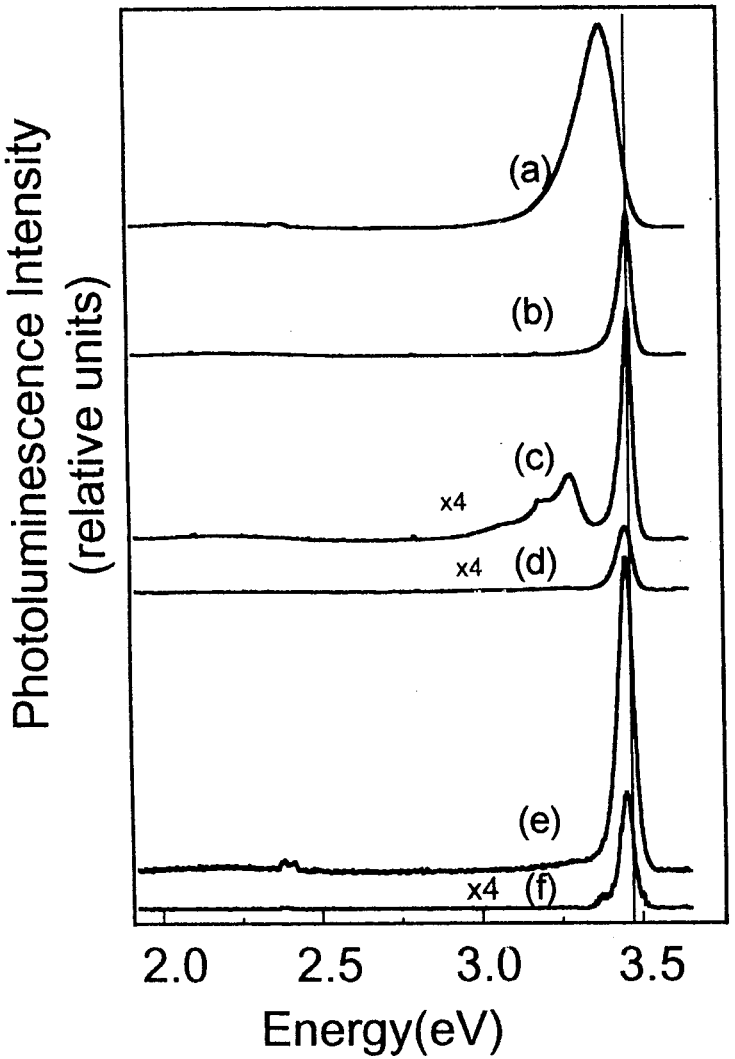

From Top to bottom

Substrate	Eg(eV)	FWHM(meV)
(a) Al_2O_3 (01.2)	3.393	144.3
(b) Al_2O_3 (11.0)	3.469	43.6
(c) Al_2O_3 (00.1)	3.469	38.7
(d) 6H-SiC	3.456	57.6
(e) Si(100)	3.456	55.7
(f) Si(111)	3.452	47.9

Conclusion:

Very narrow FWHMs mean much less carrier interaction and high quality GaN on different substrate orientations

FIGURE III-6b

results confirm the theoretical model developed at the CQD.[12] As a consequence, the research work has been principally conducted using (00•1)Al_2O_3.

GaN epilayers grown on (00•1) 6H-SiC are expected to yield improved properties because of the closer thermal and lattice match between III-Nitrides and 6H-SiC. However, due to the lower quality of the SiC substrates available at the CQD, the expected improvements have not been observed yet. The X-ray diffraction peaks generally yielded a FWHM of about 17 arcmins (Fig. III-5), which is 35 times larger than on (00•1)Al_2O_3. The near band edge luminescence at 300 K and 77 K yielded similar linewidths as on basal plane sapphire. However, by contrast to the GaN grown on other substrates, the layers on SiC did not show the deep-level associated yellow emission. The interpretation of this important feature will be one of the future work at the CQD.

High quality single crystal GaN thin films have been grown on silicon, although their quality do not compare to that on other substrates yet. Typical X-ray diffraction spectra yielded linewidths about 44 and 24 arcmins for GaN on (100) and (111)Si respectively (Fig. III-5). However, through FTIR spectroscopy of GaN on (111)Si at 300K, a sharp phonon absorption peak could be detected at 569 cm^{-1} (Fig. III-2 (bottom left)). More importantly, photoluminescence experiments showed that the GaN on silicon had as good optical quality as the layers on SiC or even (00•1)Al_2O_3. Indeed, in Fig. III-6a and III-6b, it can be seen that the linewidths of the near band edge emission were close to those of GaN on SiC and basal plane sapphire. The interpretation of the high optical quality of GaN on Si while the crystalline quality is not as good as on sapphire, still needs to be clarified and will part of the future work at the CQD.

Electrical characterization

Undoped GaN films were generally n-type, although as-grown semi-insulating GaN has been grown recently. In the conductive layers on basal plane sapphire, an electron mobility as high as 200 cm^2/Vs has been obtained, for a carrier concentration of about 10^{18} cm^{-3} at 300 K.

Conclusion and future work

First, the results presented here prove that the transfer of technology to the new low pressure MOCVD system has been successful and very fast. Secondly, the materials quality has been significantly improved compared to the materials obtained with the old MOCVD system. World-class AlN and GaN films have been achieved in a short time. Such improvements represent a major step towards the development of UV photodetectors.

Although the technology of GaN and AlN is now well established at the CQD, as well as in the rest of the research community, several issues still need to be resolved in order to fully understand the physical properties of these materials and optimize devices:

- One of the future investigation will be to understand the correlation between structural and optical quality of GaN: why much lower crystalline quality GaN layers on silicon can yield as good photoluminescence as high quality GaN on (00•1)Al_2O_3?
- Another important task will be to interpret the origin of the yellow luminescence and understand when such luminescence disappears, as in the case of GaN on SiC. It will be discussed in the following Section IV, that the introduction of dopant impurities has a significant effect in the reduction of this yellow luminescence.

References

1- S. Strite and H. Morkoç, J. Vac. Sci. Technol. **B10**, 1237 (1992)

2- H. Morkoç, S. Strite, G.B. Gao, M.E. Lin, B. Sverdlov, and M. Burns, Journal of Applied Physics 76(3), 1363 (1994).

3- *"High quality AlN and GaN epilayers grown on (00•1) sapphire, (100) and (111) silicon substrates"*
P. Kung, A. Saxler, X. Zhang, D. Walker, T.C. Wang, I. Ferguson, and M. Razeghi,
Applied Physics Letters 66(22), (May 29th 1995).

4- *"High quality aluminum nitride epitaxial layers grown on sapphire substrates"*
A. Saxler, P. Kung, C.J. Sun, E. Bigan, and M. Razeghi,
Applied Physics Letters 64(3), 339 (1994).

5- X. He and M. Razeghi, Journal of Applied Physics 73(7), 3284 (1993).

6- J. Pastrnak and L. Roskovcova, Physica Status Solidi 14, K5 (1966).

7- A.L. Holmes, K.G. Fertitta, F.J. Ciuba, and R.D. Dupuis, Electronics Letters 30(15), 1252 (1994).

8- W.E. Plano, J.S. Major, Jr., D.F. Welch, and J. Speirs, Electronics Letters 30(24), 2079 (1994).

9- M.E. Lin, B.N. Sverdlov, S. Strite, H. Morkoç, and A.E. Drakin, Electronics Letters 29(20), 1758 (1993).

10- M.S. Brandt, N.M. Johnson, R.J. Molnar, R. Singh, and T.D. Moustakas, Applied Physics Letters 64(17), 2264 (1994).

11- C. Wetzel, D. Wolm, B.K. Meyer, K. Pressel, S. Nilsson, E.N. Mokhov, and P.G. Baranov, Applied Physics Letters 65(8), 1033 (1994).

12- "*A crystallographic model of (00•1) aluminum nitride epitaxial film grown on (00•1) sapphire substrate*"
C.J. Sun, P. Kung, A. Saxler, H. Ohsato, K. Haritos, and M. Razeghi,
Journal of Applied Physics 75(8), 3964 (1994).

Photoluminescence study of GaN epilayers doped with Ge and Mg

I. Introduction

AlN, GaN and InN and their alloys cover the direct-bandgap range from 1.9eV (InN) to 6.2eV(AlN) and therefore are promising semiconductor materials for ultravoilet and blue light emitting diodes (LEDs), photodetectors and laser diodes. P-type and n-type doping have been achieved in GaN and blue LEDs have been commercially available[1]. For p-type doping, Mg has been widely used as the dopant[2,3]; for n-type doping, Si is widely used while there is only one report for Ge-doping of GaN[4].

We have reported [5] high quality AlN and GaN grown by low-pressure metal-organic chemical vapor deposition (LP-MOCVD). In this study, the photoluminescence chracterization of GaN:Mg and GaN:Ge were carried out. GaN:Ge and GaN:Mg were grown under the same conditions as in reference [5] (which was described in the previous chapters) except that doping sources were introduced. Photoluminescence spectra confirm the successful incorporation of dopants into the GaN epilayers without introducing any deep-level defects. Temperature dependent photoluminescence gives the Ge donor activation energy in GaN:Ge as 34meV, Mg-acceptor activation energy in GaN:Mg as 190meV. Ga vacancies are proposed to be the origin of the deep-level emission centered around 2.2eV in unintentionally doped GaN.

Table I. Growth Conditions of GaN:Ge and GaN:Mg

MO source	TMGa, TMAl
N source	NH_3
Ge source	GeH_4 (30ppm of GeH_4 in H2)
carrier gas	H2
substrates	Al_2O_3 (00.1), (11.0), (01.2) Si(111), (100)
buffer layer	AlN (50nm)
Growth temperature	850°C for GaN:Ge; 1000°Cfor GaN:Mg
Reactor Pressure	10mbar
Growth time	120 min

II. Experiments.

Growths were done in our AIXTRON LP-MOCVD reactor. Important growth parameters are summarized in

table 1. Cp_2Mg was used as the Mg source and GeH_4 as the Ge source. The doping level was varied by change the flow rates of the dopant sources. For photoluminescence (PL) measurements, a He-Cd laser (325nm) with an output power of 10mW was used as the excitation source. Temperature-dependent measurements from 77K to 300K were carried to find out the possible origins of emission peaks and activation energies of Ge and Mg.

III. Results and discussion.

(i). Ge-doped GaN.

In this study, the GaN:Ge layer was grown on basal plane sapphire and has a room temperature electron concentration of $10^{20}cm^{-3}$, a mobility of $30cm^2/V.s$. The surface is smooth and free from cracks. The much higher electron concentration of GaN:Ge verifys that Ge is a donor, which substitutes Ga sites. Figure 1 shows PL at 77K and room temperature. At 77K, three peaks were observed from strongest to weakest: 3.35eV, 3.31eV and 3.24eV. They are below the bandgap of GaN (3.47eV) and thus must be from Ge-donor related transitions. An interesting and important observation is that no deep-level emission was observed.

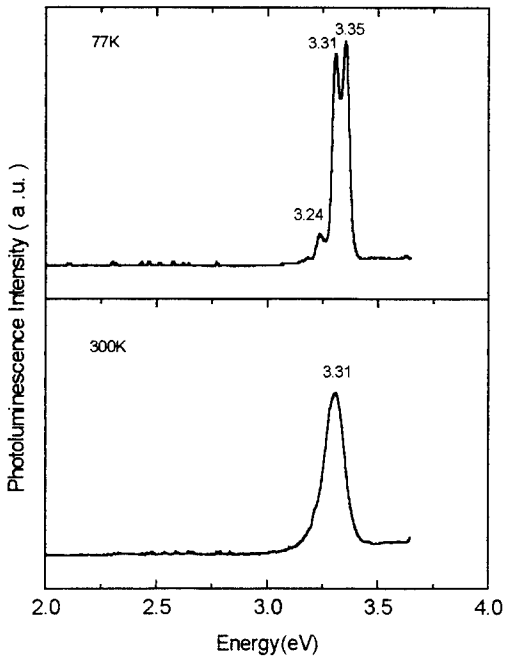

Fig.1 Room temperature and 77K PL of Ge-doped GaN.

To find the possible origins of these emissions, we did a temperature dependent PL from 77K to 300K. The evolution of the peak energies and the peak intensity of the strongest peak is shown in Fig. 2 and Fig. 3 respectively. The following results were obtained:

(1). The 3.35eV peak follows the bandgap of GaN while the 3.31eV and 3.24eV peak is essentially temperature independent form 77K to 180K (Fig.2). The similar

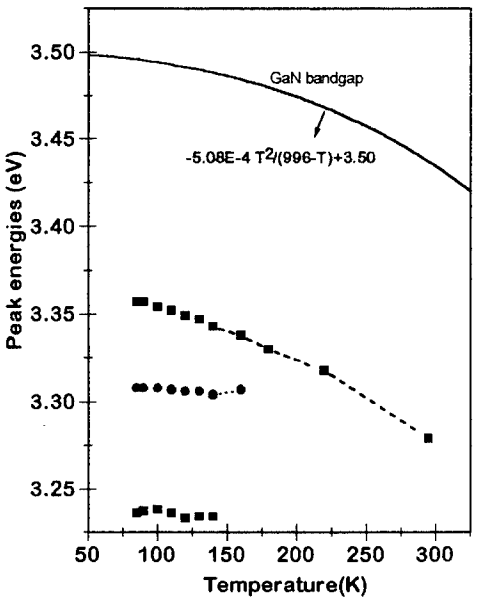

Fig.2. Shift of PL peak energies with temperature variation. Bandgap energy of GaN is also shown for comparison.

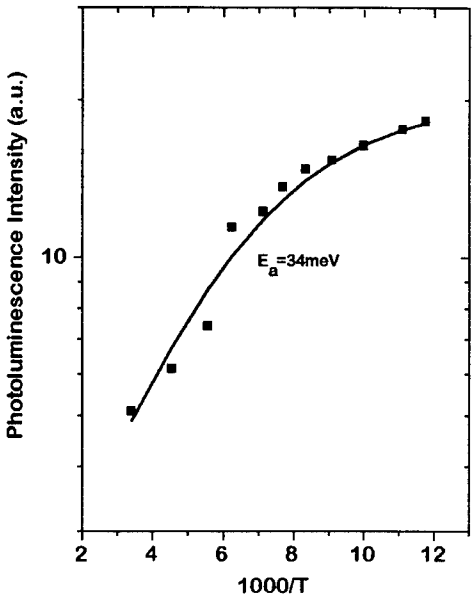

Fig.3 The 3.35eV Peak intensity as a function of temperature. The fitting function is shown as the solid curve.

behaviors of the 3.31eV peak and the 3.24eV peak suggests that they are from the same origin. Their distance is ≈ 70meV or 570cm^{-1} and the intensity of 3.24eV peak is much weaker, which suggests that the 3.24eV peak is a phonon replica of the 3.31 emission. The phonon mode is the E_1(TO) mode of GaN[6].

(2). The PL intensity from an impurity related emission can be described by the following function [7]:

---

where I(0), I(T) is the PL intensity at 0°K and T °K respectively, C is a constant, E_a is the activation energy of the impurity, k is the Boltzmann constant. Fitting the data in Fig. 3 to the function we obtained an activation energy of 34meV for Ge-donor level, which is

very close to the estimation of Lagerstedt[8] and Dingle et .al. [9] and thus confirm Ge as a donor has been successfully incorporated into the GaN layer.

From the above results, we tentatively assigned the 3.35eV and 3.31eV are Ge-donor to different acceptors recombinations and the 3.24eV peak is the TO-phonon replica of the 3.31eV D-A recombinations. These peaks should not be from the phonon replicas of either I_1 line (emission of exciton bound at neutral acceptor sites) or I_2 line (emisson of exciton bound at neutral donor site) of GaN[9] because both of them are not observed here. The temperature-independent characteristic of the 3.31eV D-A recombination and its phonon replica might partly be explained by the electron kinetic energy correction, which account for[8] about half of the shift expected. Low energy phonon interaction could also influence the peak position.

(ii). Mg-doped GaN.

Figure 4 shows the 77K PL of as-grown GaN:Mg on basal plane sapphire. It is very similar to PL spectra of GaN:Mg observed by other research groups [10]. The 3.27eV peak and its lower enery satellite peaks have been confirmed to be donor-to-(Mg) acceptor (D-A) recombination and its phonon replicas[10].

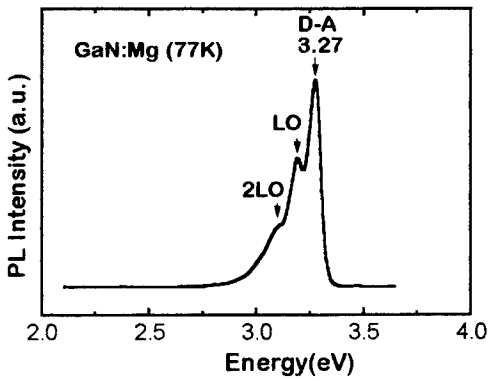

Fig.4 PL of GaN:Mg at 77K

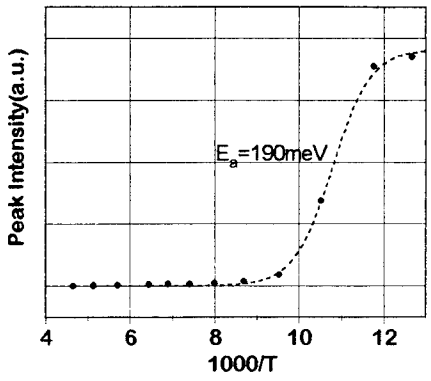

Fig.5 D-A recombination peak intensity as a function of temperature. E_a=190meV is obtained

Various authors have reported the activation energy of Mg in GaN:Mg with values of 125meV[11], 155-165meV[11,12] and 190meV[13] . We also performed a temperature dependent PL study of the D-A emission in our semi-insulating GaN:Mg. The temperature variation of the peak intensity is shown in Fig. 5. Using the same curve fitting process as described above for the Ge-donor, we obtained an activation energy of 190meV for Mg acceptor in GaN:Mg.

GaN:Mg on other substrate orientations showed similar PL spectra. Figure 6 shows the FTIR (Fourier Transform Infrad) absorption spectum (at 300K) of this sample. A sharp and strong phonon peak at 564cm^{-1} can be clearly observed. This phonon mode is the E_1(TO) mode of GaN. It suggested that the high quality of the GaN is not perturbed by the Mg-doping.

An interesting and important observation is that no deep-level emission was observed in all GaN:Mg samples.

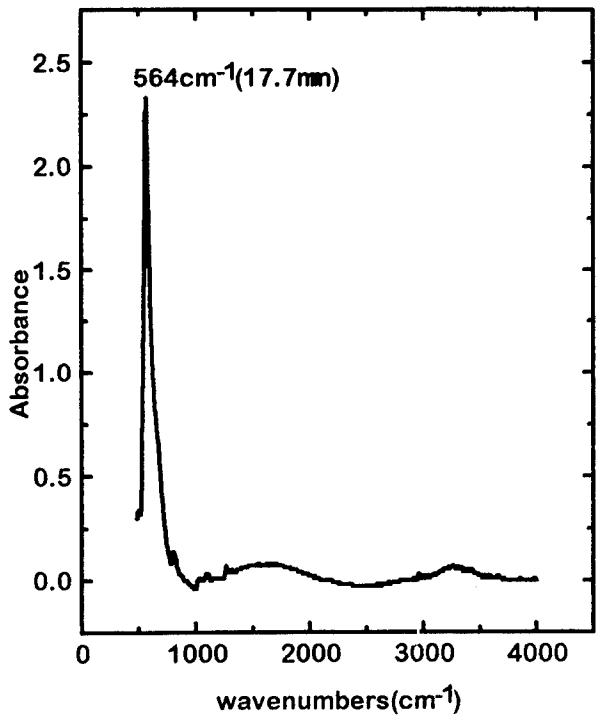

Fig. 6. FTIR absorbance of GaN:Mg on Si (111) substrate, which showed similar PL to Fig.4. The phonon mode observed is the E1(TO) mode of GaN.

IV. Conclusion and future work.

From the photoluminescence study of GaN:Ge and GaN:Mg, we conclude that Ge and Mg have been successfully incorporated into GaN. An important observation is that

no deep-level emission was observed from GaN:Mg and GaN:Ge, which strongly suggests that the deep-level yellow emission appears at around 2.2eV in undoped GaN is from the Ga vacancies because both Mg and Ge substitute the Ga sites.

We have shown some preliminary results for p-type and n-type doping of GaN with Mg and Ge. Because of problems of reactor recently, we were not able to continue this study. In the future, we plan to increase the doping level of Mg in GaN and improve the controllability of n-type doping of GaN with Ge or Si, which is also available in our reactor. As-grown GaN:Mg were semi-insulating, post-growth annealing is being carried out in an effort to activate the Mg-level. Low-energy electron beam irradiation (LEEBI) treatment is also accessible for us and will also be carried out.

Reference

[1] S. Nakamura, T. Mukai, and M. Senoh, J. Appl. Phys. **76**, 8189(1994).

[2] H. Amano, M. Kito, K. Hiramatsu, and I. Akasaki, Jpn. J. Appl. Phys., **28**, L2112(1989).

[3] S. Nakamura, T. Mukai, M. Senoh, and I. Iwasa, Jpn. J. Appl. Phys., **31**, L139(1992).

[4] S. Nakamura, T. Mukai and M.Senoh, Jpn. J. Appl. Phys. **31**, 2883(1992).

[5] P. Kung, A. Saxler, X. Zhang, I. Ferguson and M. Razeghi, to be published on May in Appl. Phys. Lett.

[6] T. Kozawa, T. Kachi, H. Kano, Y. Taga, M. Hishimoto, N. Koide and K. Manabe, J. Appl. Phys. **75**, 1098 (1994)

[7] J. Pankove, Optical Processes in Semiconductors, Dover Publications Inc., New York.

[8] O. Lagerstedt and B. Monemar, J. Appl. Phys. **45**, 2266 (1973).

[9] R. Dingle, D. D. Sell, S. E. Stokowski and M. Ilegems, Phys. Rev. **B4**, 1211 (1971).

[10] H. Amano, M. Kitoh, K. Hiramatsu and I. Akasaki, J. Electrochem. Soc.**137**, 1639(1990).

[11] T. Tanaka, A. Watanabe, H. Amano, Y. Kobayashi, I. Akasaki, S. Yamazaki and M. Koike, Appl. Phys. Lett. **65**, 593(1994).

[12] I. Akasaki, H. Amano, M. Kito and K. Hiramatsu, J. Lumin. **48&49**, 666 (1991).

[13] M. Ilegems and R. Dingle, J. Appl. Phys. **44**, 4234 (1973).

Tenary Compound Growth of $Al_xGa_{1-x}N$ and $Al_xGa_{1-x}N$:Ge

I. Introduction.

$Al_xGa_{1-x}N$ is an excellent candidate for various ultraviolet (UV) electro-optic devices in the spectral range of 200nm - 300 nm. The UV spectrum could be covered by $Al_xGa_{1-x}N$ based tunable light-emitting diodes (LEDs), laser diodes (LDs) and photodetectors by controlling the solid composition. Its direct wide bandgap and potential of heterojunction fabrication[1] make it a good choice for highly efficient UV-photodetectors. Like most wide bandgap semiconductors, these photodetectors are expected to exhibit superior radiation hardness compared to GaAs or Si-based photodetectors. This makes them attractive for space application especially in the technologically significant region 240nm- 280nm, where absorption by ozone makes the earth's atmosphere nearly opaque.

We reported the growth of $Al_xGa_{1-x}N$ with our atmospheric pressure MOCVD reactor[2]. In this study, By using our low-pressure MOCVD reactor, the growth of $Al_xGa_{1-x}N$ from x=0 to x=1 on Al_2O_3 (00.1) and Si(111) substrates and the Ge-doping of $Al_{0.2}Ga_{0.8}N$ on sapphire substrate were carried out. This paper reports the following results: (i).Room temperature UV absorption of $Al_xGa_{1-x}N$ and $Al_xGa_{1-x}N$:Ge; (ii) Room temperature and 77K photoluminescence measurements of $Al_{0.2}Ga_{0.8}N$. (iii) Electrical properties of $Al_xGa_{1-x}N$ and $Al_{0.2}Ga_{0.8}N$:Ge. These characterization results confirm that our $Al_xGa_{1-x}N$ epilayers are of high quality. This is also the first report of Ge-doping of $Al_xGa_{1-x}N$ and the Al composition (x=0.2) of the $Al_xGa_{1-x}N$ in which we achieved successful n-type doping is the highest up to date.

II. Experiments

A horizontal-type MOCVD reactor operated at low pressure was used for the growth of $Al_xGa_{1-x}N$ and $Al_xGa_{1-x}N$:Ge. Table I summarizes the important growth conditions. To reduce parasitic pre-reaction in the gas phase, the MO sources and the NH_3 were mixed just before the susceptor. In each growth, sapphire and silicon substrates were put on the susceptor side by side. The susceptor was spun at a speed of 30ppm by a

gas foil rotation technique. As a result, the epilayers were very uniform, transparent and free from cracks. The Al composition is varied by changing the flow ratios of TMAl and TMGa.

All samples were characterized by UV absorption (or transmission) to determine the bandgap. The UV absorption was done in a Varian Cary-13E dual-beam UV spectrometer from the wavelength of 190nm - 900 nm (6.53eV to 1.4eV). A clean substrate was put in the reference path and the sample was put in the measurement path. Thus the product of the absorption coefficient and the thickness of the epilayer was directly obtained from the spectrometer. Photoluminescence measurements were carried out at room temperature as well as 77K. The excitation source was a He-Cd laser whose wavelength is at 325nm and output power is 10mW. Because of the energy limitation of this laser, only $Al_xGa_{1-x}N$ alloys with $x<0.1$ on sapphire and silicon were characterized. X-Ray diffraction was performed with a Phillips Research Laboratories high resolution five-crystal diffractrometer. The phonon modes of the alloys were determined by Fourier Transform Infrad (FTIR) absorption at room temperature, which was done in a Galaxy 3000 series FTIR spectrometer. Electrical measurements was done in a Bio-Rad Hall measurement system with Van der Paul method.

Table I. Growth Conditions of $Al_xGa_{1-x}N$

MO source	TMGa, TMAl
N source	NH_3
Ge source	GeH_4 (diluted with H2)
carrier gas	H2
substrates	Al_2O_3 (00.1), Si(111)
buffer layer	AlN (50nm)
Growth temperature	850C
Reactor Pressure	100mbar
Growth time	120 min

III. Undoped $Al_xGa_{1-x}N$.

(i) Optical Characterizations and results.

For the absorption of direct bandgap materials, the absorption coefficient α is determined by[3]

$$\alpha = A(h\nu - E_g)^{1/2}$$

where A is a constant, hν is the energy of the incident light and E_g is the bandgap energy. The above equation gives $\alpha^2 = A^2(h\nu - E_g)$ or $(\alpha t)^2 = (At)^2(h\nu - E_g)$ where t is the thickness of the layer. This suggests a linear relation between $(\alpha t)^2$ and hν in the

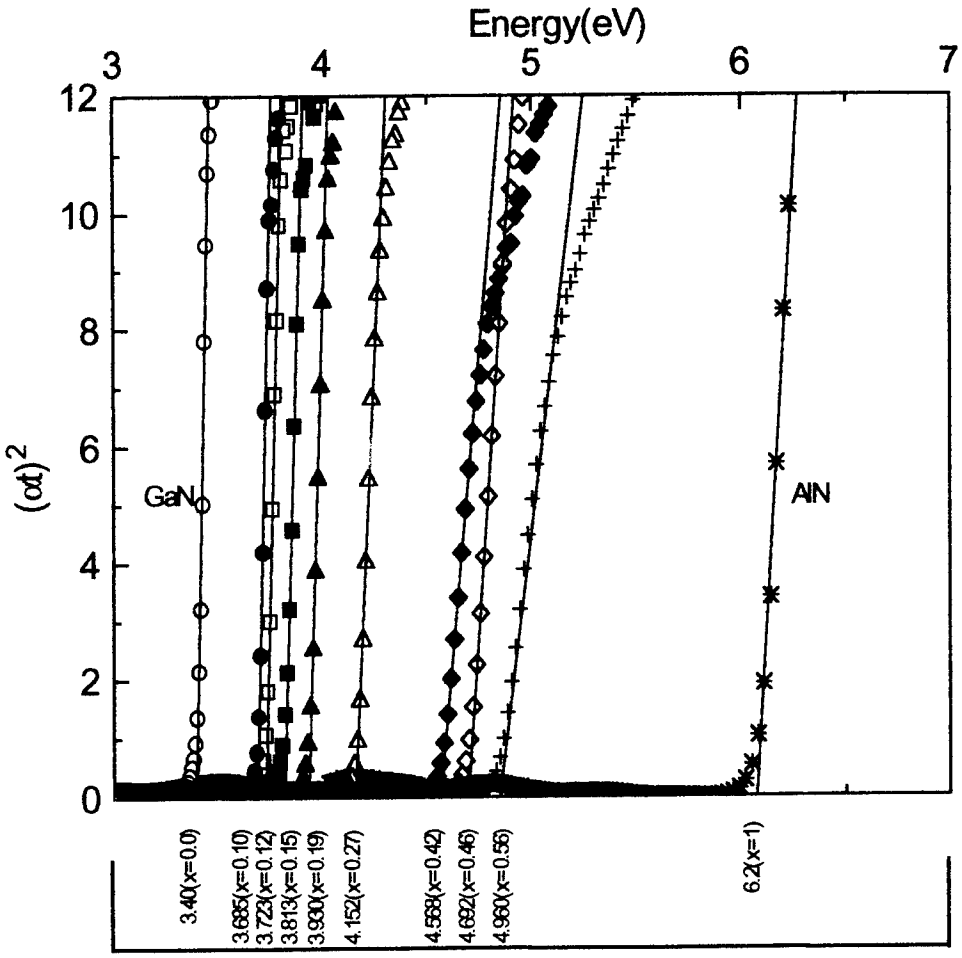

Fig.1 Bandgap absorption edge of AlxGa1-xN. UV absorption were done at room temperature.

absorption edge. Figure 1 shows the square of the product of the absorption coefficient and the thickness $(\alpha t)^2$ as a function of the incident photon energy hν in the whole range from x=0 to x=1. The effect of the AlN buffer layer on the absorption (or transmission) of $Al_xGa_{1-x}N$ with x <1 are neglected since the AlN is very thin and transparent for energy lower than the bandgap of AlN 6.2eV. To reduce the overlap between different curves, only the bandedge absorption areas are shown here. From the linear fitting of the

absorption edges in Fig.1, the bandgap energies are determined. Two points are obvious from the figure: (i). The bandgap edge absorption curves show a very good linear dependence on the photon energy hν , which confirms the $Al_xGa_{1-x}N$ alloy is of direct bandgap; (ii). The curves near the absorption edge show no tail up the lower energy sides which suggests high optical quality of the epilayers. The lower energy tail near the absorption edge reported by Koide et.al[4] and Hagen[5] et.al. may suggest phonon assisted absorption.

Several authors[4,6] reported the dependence of bandgap energy on the Al composition showed that the bandgap energies of $Al_xGa_{1-x}N$ alloys follows a linear relation with slightly bowing. As a good approximation, we assume a linear relation and estimated the Al compositions on epilayers grown on sapphire substrate. which are also shown in Fig.1. As for the composition of Al on epilayers grown on silicon substrates, because silicon opaque in the UV range, it is not possible to obtain bandgap energy from UV transmission. We are trying to obtain Al composition by using electronprobe microanalysis (EPMA or EDAX). Before that, we roughly assume that the Al compositions of epilayer grown on silicon are the same as those on sapphire in the same growth, which is verified by the photoluminescence measurement described below.

Figure 2 show the transmission spectra of $Al_xGa_{1-x}N$ layers. Fabry-Perot oscillations were observed on all layers and this confirm the epilayer is uniform and smooth.

Figure 3 shows a complete absorption curve for $Al_{0.17}Ga_{0.83}N$ at room temperature. It can be seen that the absorption follows the $\alpha = A(h\nu - E_g)^{1/2}$ very closely.. The oscillation at energies lower than bandgap might be due to reflection because it was not taken into account in the measurement At energies higher than bandgap, compare to the effect of absorption, the effect of the reflection is small enough to be negligible. However, at very high

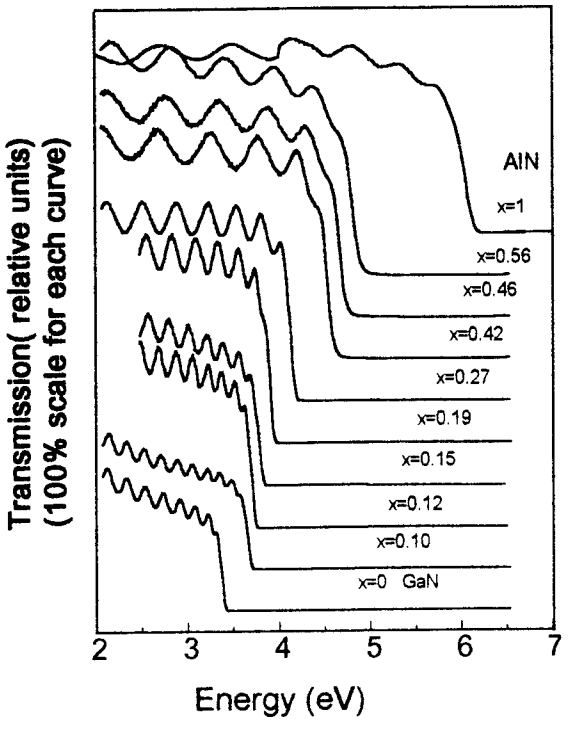

Fig. 2 UV transmissions of AlxGa1-xN. Sharp cut-off and Fabry-Perot fringes show high quality of the epilayers

energies, the absorption is so high that the transmitted signal received by the detector is very weak. This generated some error at high energy side.

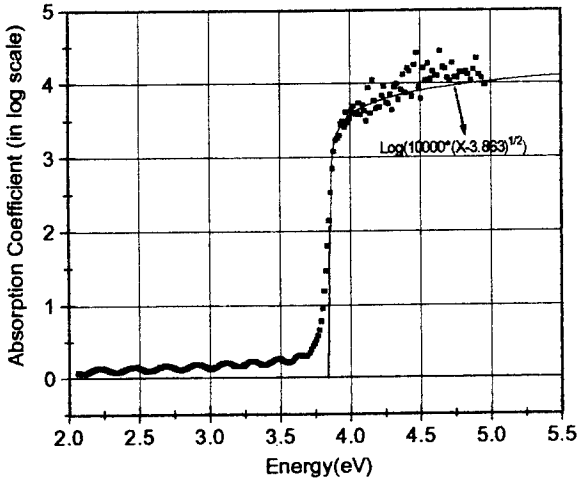

Fig. 3 UV Absorption curve of $Al_{0.17}Ga_{0.83}N$ with its function curve fitting

The Compositions of Al in all samples were further calculated from the lattice constants which were obtained from X-Ray diffraction measurements, assuming a linear relation between the lattice constant and the Al composition of the alloys. Figure 4 shows the Al composition x of $Al_xGa_{1-x}N$ obtained from energy bandgap and lattice constant. it can be seen that the composition obtained from lattice constant is close to that obtained from bandgap but with some variations, which might be due to compositional variations in the layers or due to different carrier concentration (see Ge-doped samples).

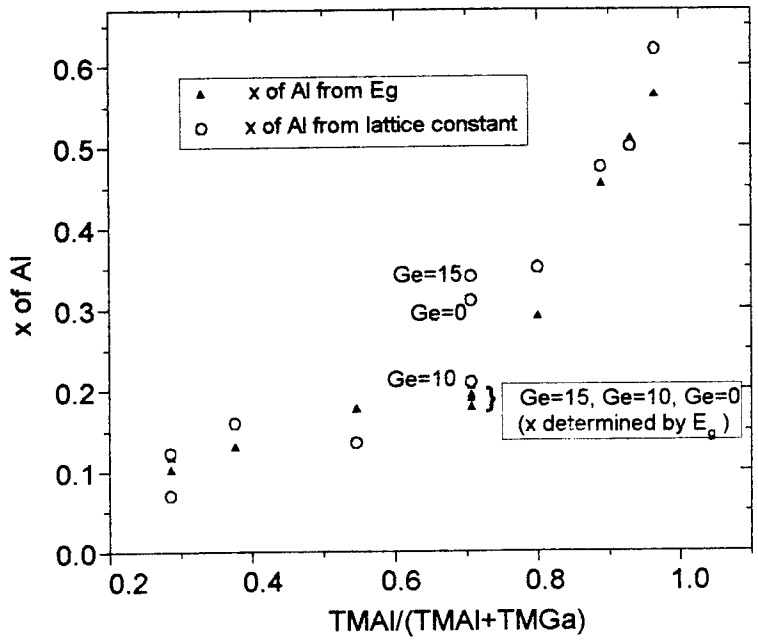

Fig. 4 Composition of Al in $Al_xGa_{1-x}N$ determined from bandgap energy of lattice constant. Vegard's law is assumed for both cases.

The room temperature and 77K photoluminescence of $Al_{0.1}Ga_{0.9}N$ on basal plane sapphire substrate and (111) silicon are shown in Fig.5

and Fig.6 respectively. Both of these two figures show that emission peak energies have been shifted to higher energy compared to GaN edge emission and thus confirm the successful growth of $Al_xGa_{1-x}N$. Room teperature PL showed efficient bandedge emission with small deep-level emission. There are three interesting points to be noticed in these two PL spectra: (i) the deep-level emission was also shifted to higher energy, which suggests that the deep level emission is also related to the bandgap or shallow acceptor or shallow donor; (ii) the two samples measured here were from the same growth. It can be seen that the difference between their PL emission peak energies are very small. This partly support our assumption that the Al composition of $Al_xGa_{1-x}N$ on Si(111) and Al_2O_3(00.1) from the same growth is approximately the same. The small difference may

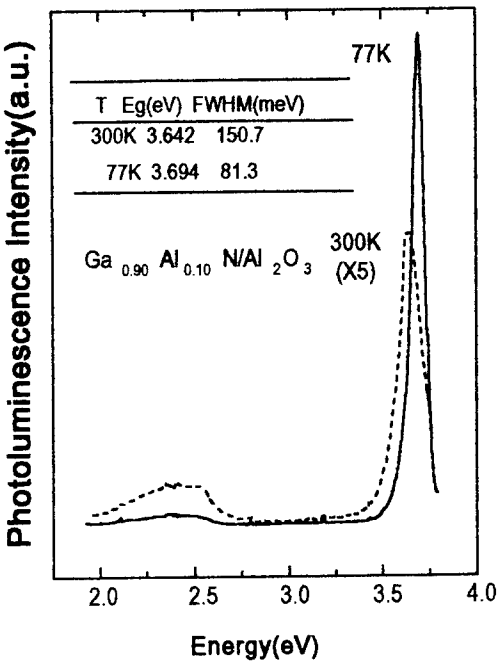

Fig.5 Room temperature and 77K PL of $Al_{0.1}Ga_{0.9}N$ on sapphire (00.1) substrate

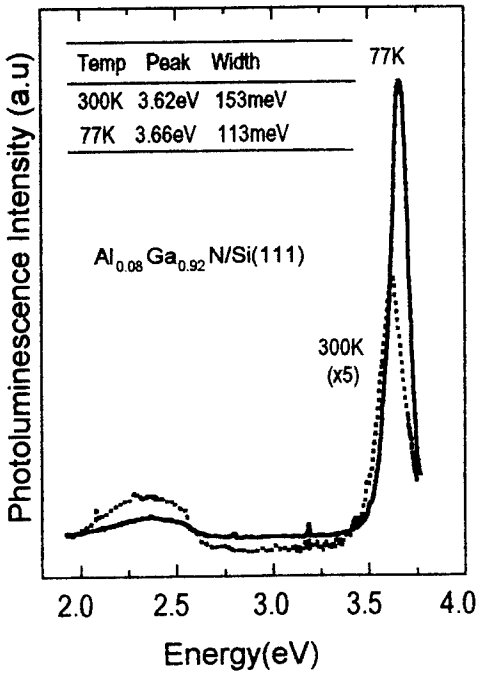

Fig.6 Room temperature and 77K PL of $Al_{0.1}Ga_{0.9}N$ on silicon(111) substrate

indicate the Al incorporation in $Al_xGa_{1-x}N$ on Si is slightly less efficient than that on Al_2O_3 substrate. EPMA has to be performed to verify these assumptions.

Figure 7 shows the evolution of phonon modes with the solid composition x in $Al_xGa_{1-x}N$ alloys on Si(111). Here the $E_1(TO)$ and $A_1(TO)$ phonon mode is studied. As can be seen in the figure, the frequency of each phonon mode increases with increasing solid composition x, but they do not obey the linear interpolation between GaN and AlN (which is shown as lines in the figure). Similar results were reported by Hayashi et.al.[7] with Raman spectroscopy but only up to x=0.15.

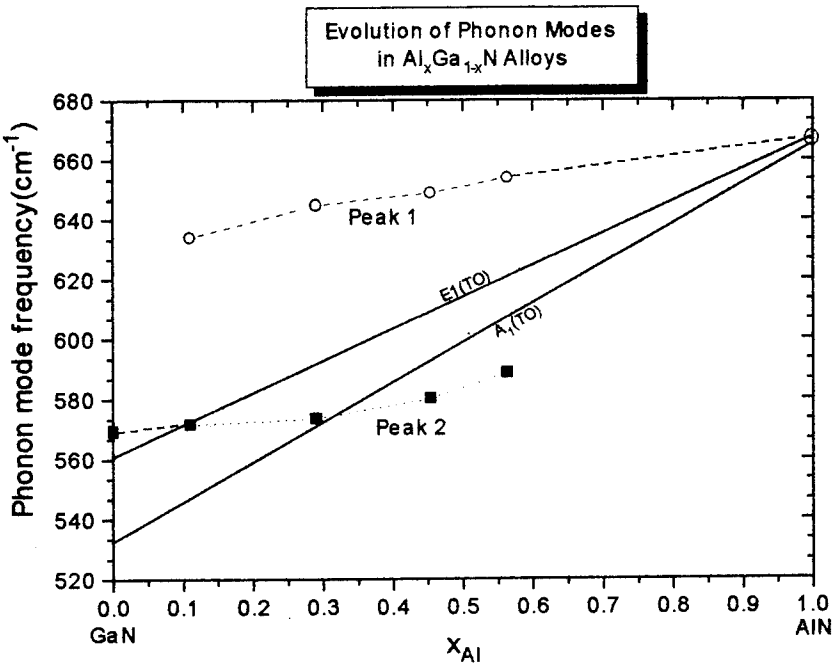

Fig. 7 Frequency of Phonon modes in AlxGa1-xN on Si as a function of Al composition. The two solid lines are the linear interpolations between the A1(TO), E1(TO) mode observed in GaN and these modes observed in AlN.

(ii) Electrical measurements.

The resistivity and carrier concentration of the as-grown $Al_xGa_{1-x}N$ on sapphire substrates up to x=0.2 were measured and shown in Fig.8. All samples measured exhibited n-type conductivity. The layers with x>0.27 are so highly resistive that we could not measure them. From Fig.8 it can be seen that with the increase of the Al composition x, the resistivity increase exponentially while the concentration increases linearly (notice that Log scale is used for vertical axis's). Similar study was reported by Yoshida et. al.[6] but their results are different from us in three aspects : (i). With the increase of Al composition, the carrier concentration and the resistivity of our samples increase more rapidly than that of their samples. (ii). For the same Al solid composition, carrier concentration in our sample is almost two orders magnitude lower than theirs. The much lower carrier concentration in our samples suggests higher purity.

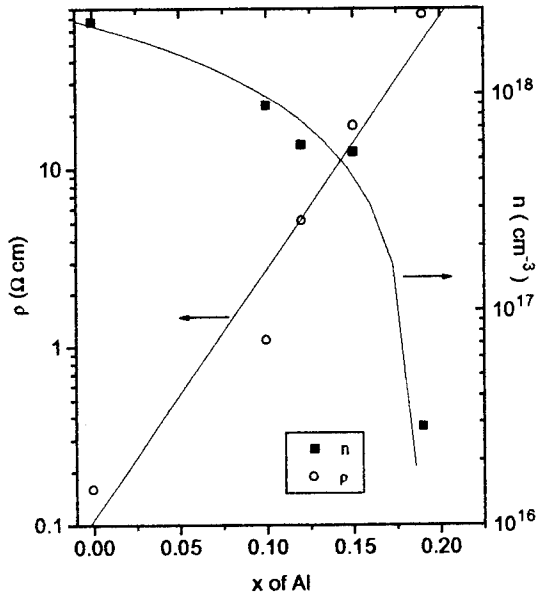

Fig. 8. Resistivity and carrier concentration of $Al_xGa_{1-x}N$ up to x=0.2. Log scale for vertical axis's.

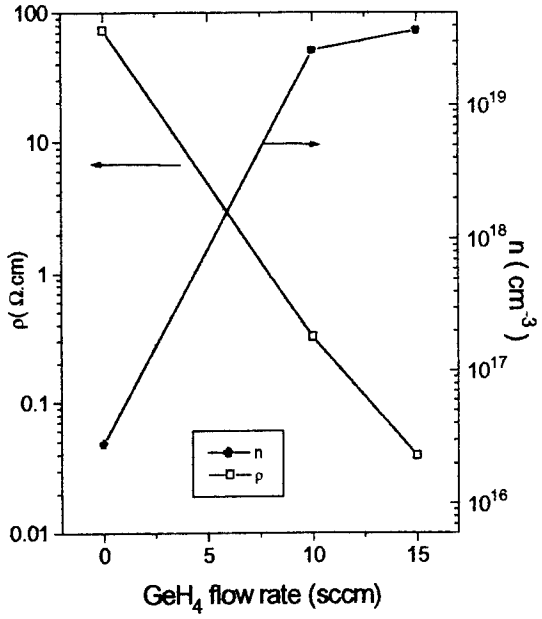

Fig.9.Resistivity and carrier concentration of $Al_xGa_{1-x}N$:Ge linear scale is uesd scale to show the linear relationship.

IV. Ge-doped $Al_{0.2}Ga_{0.8}N$.

Doping of $Al_{0.1}Ga_{0.9}N$ with Si was reported by Murakami et. al. [8]. They obtained n-type carrier concentration up to $2x10^{18}$ cm^{-3} without cracks in the epilayers. In our study here, with such low carrier concentrations in as-grown $Al_{0.2}Ga_{0.8}N$. we were able to doped it with Ge very efficiently. We obtain concentrations as high as $3.7x10^{19}cm^{-3}$ while maintaining a smooth surface and good morphology. The undoped $Al_{0.2}Ga_{0.8}N$ has a carrier concentration of $2\times10^{16}cm^{-3}$ and a resistivity of 73 Ωcm (see figure 8). Figure 9 shows the resistivity ρ and the free electron concentration n of $Al_{0.2}Ga_{0.8}N$:Ge as a function of GeH_4 flow rate. It can be clearly seen that the resistivity ρ was significantly reduced and the free electron concentration n is greatly increased after Ge doping. It also strongly indicated that Ge acts as a donor in the $Al_{0.2}Ga_{0.8}N$ layer.

UV absorption showed that the bandgap is not shifted after Ge-doping while free carrier absorption is increased.

V. Conclusions and future work.

Growth and properties of $Al_xGa_{1-x}N$ and $Al_xGa_{1-x}N$:Ge by LP-MOCVD using AlN buffer layer have been studied in detail. The very low carrier concentration, sharp UV absorption edge and room temperature photoluminescence show that $Al_xGa_{1-x}N$ is of high quality. Efficient n-type doping of $Al_xGa_{1-x}N$ has been achieved by using GeH_4 as the source gas. It is strongly suggested that Ge acts as a donor in $Al_xGa_{1-x}N$ and replaces group-III (Ga or Al) lattice sites.

p-type doping of $Al_xGa_{1-x}N$ with Mg will be carried out in the future. It is expected that with such low carrier concentration, Mg-doping of $Al_xGa_{1-x}N$ would be easier to achieve than Mg-doping of GaN, which usually shows a n-type background carrier concentration of 10^{18} cm^{-3}. The controllability of n-type doping will be studied by reducing the GeH4 flow. N-type doping of AlxGa1-xN with higher Al composition (up to Al) will be carried out. After these, p-n junction will be grown and fabricated. P-i-n junction UV photodetectors are expected to be demonstrated at that time.

References:

[1] M. A. Khan, R. A. Skogman, J. M. van Hove, S. Krishankutty and R. M. Kolbas, Appl. Phys. Lett. 56, 1257 (1990).

[2] C. J. Sung, P. Kung, A. Saxler, H. Ohsato and M. Razeghi, Inst. Phys. Conf. Ser. 137, Chapt. 4, 1993.

[3] J. I. Pankove, Optical Processes in Semiconductors, Dover Publications Inc., New York, 1971.

[4] Y. Koide, H. Itoh, M. R. H. Khan, K. Hiramatsu, N. Sawaki and I. Akasaki, J. Appl. Phys. 61, 4540, 1987.

[5] J. Hagen, R. D. Metcalfe, D. Wickenden and W. Clark, J. Phys., C11, L143 (1978).

[6] S. Yoshida, S. Misawa and S. Gonda, J. Appl. Phys. 53, 6844 (1982).

[7] K. Hayashi, K. Itoh, N. Sawaki and I. Akasaki, Solid State Commun. 77, 115 (1991).

[8] H. Murakami, T. Asahi, H. Amano, K. Hiramatsu, N. Sawaki and I. Akasaki, J. Cryst. Growth 115, 648 (1991).

VI. UV PHOTODETECTORS

Introduction

As discussed in the introduction (Section I), the $Ga_{1-x}Al_xN$ alloy system is the most promising material for the future UV photodetector technology because III-Nitride-based devices will be capable of improved high-power and -temperature operation due to their large bandgaps and chemical stability. Schottky barrier devices and photoconductors are most frequently used for wide bandgap semiconductor UV photodetectors. Photoconductors offer the important advantages of internal photoelectric gain which relaxes the requirement for a low noise preamplifier. Lightly doped and long majority lifetime materials have to be used in order to obtain a better signal to noise performance. To date, there have been few reports on experimental UV photodetectors using GaAlN.[1,2] To the best of our knowledge, the excess carrier lifetime has never been determined in this material system.

The first step towards the development of GaN and GaAlN photoconductors include:

- the development of techniques to measure photoconductive lifetime τ in III-Nitrides,
- the measurement of photoconductive lifetimes,
- the correlation between these lifetimes and the other physical properties of the materials,
- the prediction of the performance of UV photoconductors as predicted from lifetime measurements.

All these measurements have been conducted successfully with a very simple setup which will be described in the next paragraph. The CQD is currently realizing a complete homemade UV-measurement apparatus which will allow to measure the UV transmission/absorption, UV reflectance, UV spectral response of GaAlN detectors (see last paragraph of this section).

Samples and measurement apparatus

Since the purpose of this study has been to correlate the photoconductive lifetimes and the physical properties of the III-Nitride layers, a wide range of films with different electrical quality needed to be characterized. To date, two n-type GaN and a n-type $Ga_{0.93}Al_{0.07}N$ samples have been characterized. They consisted of an active layer on top of an AlN buffer layer. They have been clover-patterned with indium pads have been soldered on the four corners of the pattern, in order to realize a Van der Pauw configuration (Fig. VI-1).

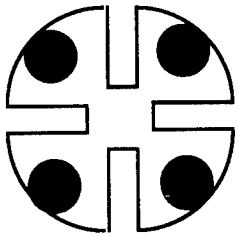

Fig. VI-1. Clover pattern.

The electrical properties of the materials at 300 K have been determined by Hall measurements on the patterned samples. The parameters for the three chosen samples are summarized in the following Table VI-A.

Sample #	Thickness (μm)	ρ (Ωcm)	μ_e (cm^2/Vs)	n ($x10^{17}$ cm^{-3})
GaN #1	1.6	0.0252	143	17.3
GaN #2	1.36	0.693	25	3.61
$Ga_{0.93}Al_{0.07}N$	1.465	1.14	5.69	9.62

Table VI-A. Physical parameters for the 3 chosen samples.

One original way to characterize the photoconductivity of III-Nitrides is to use this same Van der Pauw configuration. Two neighbor contacts are biased by an external voltage supply, while the two others are used to measure the photoconductive signal (Fig. VI-2). Such configuration eliminates the influence of contact effects, such as contact resistance, photovoltaic effects and others, on the photoconductivity measurements. The excitation source is the same as the one used for photoluminescence: a He-Cd laser, emitting at 325 nm, with a DC output power of about 10 mW. The sample were front-side illuminated.

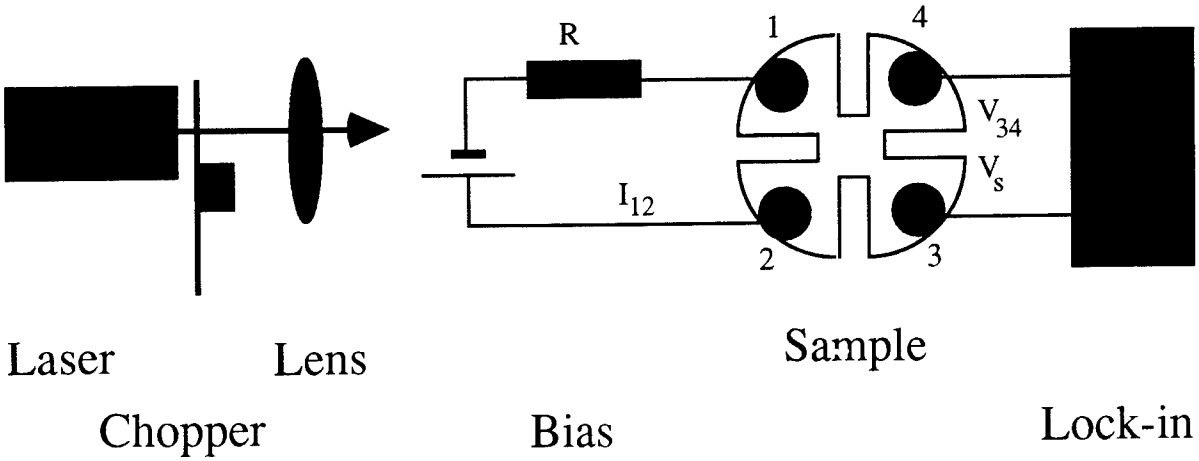

Fig. VI-2. Geometry and electrical circuit for photoconductivity measurement.

Van der Pauw configuration in photoconductivity measurements

It can be shown that for the symmetrical structure shown in Fig. VI-2, the resistivity ρ can be determined from the following relation:

$$\rho = \frac{\pi t}{\ln 2}\frac{V_{34}}{I_{12}} = 4.532t\frac{V_{34}}{I_{12}} \qquad (1)$$

where t is the thickness of sample. The sheet resistance R_{sh} will then be:

$$R_{sh} = \frac{\rho}{t} = 4.352\frac{V_{34}}{I_{12}} \qquad (2)$$

Estimation of photoconductive lifetime

In the following discussion, it will be assumed that the sample is constant-current biased by I_{12} and uniformly illuminated. Equilibrium conditions, ie: weak excitation and stationary conditions (in which the frequency of excitation is $<< 1/2\pi\tau$), will also be assumed. This translates into: $\Delta n << n_0$, the equilibrium carrier concentration. Consequently, the photosignal voltage V_s at contacts 3-4 will be small compared to the dark voltage V_{34}, and the change in sheet resistance ΔR_{sh} will also be small compared to the sheet resistance R_{sh}. It can be shown that:

$$V_s = \frac{I_{12}}{4.532}\Delta R_{sh} = V_{34} R_{sh} \Delta G_{sh} \qquad (3)$$

The change in the detector sheet conductance ΔG_{sh} can be expressed in terms of the excess carrier concentration (n-type assumed) per unit area ΔN_{sh}:

$$\Delta G_{sh} = q \mu_e \Delta N_{sh} \qquad (4)$$

The excess carrier lifetime can be defined by the equation:

$$\tau = \frac{\Delta N_{sh}}{g_{sh}^{op}} \qquad (5)$$

where g_{sh}^{op} is the optical generation rate per unit of area which is equal to $g_{sh}^{op} = \eta\Phi$, η being the quantum efficiency and Φ the photon flux density. Assuming that the recombination lifetime is independent on excitation level, the change in sheet conductance is:

$$\Delta G_{sh} = q\mu_e \tau\eta\Phi \tag{6}$$

For monochromatic excitation radiation, Φ is given by:

$$\Phi = \frac{\lambda P}{hc} \tag{7}$$

where P is the optical power density.

Therefore, by combining Eqs. (3), (6) and (7), the photovoltage signal V_S becomes:

$$V_S = V_{34} R_{sh} q\mu_e \tau\eta \frac{\lambda P}{hc} \tag{8}$$

Expressed V_{34} and R_{sh} in terms of the materials electrical parameters, Eq. (8) becomes:

$$V_S = \frac{I_{12}\rho^2}{4.532t^2} q\mu_e \tau\eta \frac{\lambda P}{hc} \tag{9}$$

and the photoconductivity lifetime is given by:

$$\tau = \frac{4.532t^2}{I_{12}} \frac{1}{\rho^2 q\mu_e} \frac{hc}{\eta\lambda P} V_S \tag{10}$$

Consequently, the measurements of the photoconductivity response can be used to determine the effective photoconductivity lifetime.

Assuming internal quantum efficiency of ≈1, the quantum efficiency η has been calculated using:

$$\eta = (1-r)\frac{(1-e^{-\alpha t})}{(1-re^{-\alpha t})} \tag{12}$$

where r is the reflection coefficient and t is the film thickness.

Estimation of photelectric gain, current and voltage responsivities

The measurement of the effective photoconductivity lifetime allows to calculate the photoelectric gain, voltage and current responsivities of photoconductors prepared from the same material.

According to the simple theory of photoconductivity the photoelectric gain is:

$$g = \frac{\tau}{t_t} \tag{13}$$

where t_t is the transit time of the majority carriers between contacts. In terms of the electrical parameters of the materials, the gain in the linear regime (not saturated carrier velocity) is:

$$g = \frac{\tau \mu_e V}{l^2} \tag{14}$$

where l is the distance between the contacts and V is bias voltage.

The current and voltage responsivities are respectively given by:

$$R_i = \frac{q\lambda}{hc}\eta\frac{\tau \mu_e V}{l^2} \tag{15}$$

$$R_v = \frac{q\lambda}{hc}\eta\frac{\tau \mu_e V}{l^2}R_d \tag{16}$$

where l is the detector length, V is the bias voltage, and R_d is the device resistance.

Photonductivity measurements

These measurements have been conducted using the Van der Pauw configuration described earlier. The electrical parameters of the samples are given in Table VI-1. In view of the resistivities of the samples, a load resistance of 592 kΩ has been used in the biasing circuit to ensure a constant-current condition. The biasing voltage has been adjusted to obtain a strong signal.

Three experimental parameters influence photoconductivity measurements and had to be taken into account: the bias voltage, the excitation power and frequency.

Bias voltage

For a set excitation power and frequency, the photosignal showed the expected linear relationship versus the bias voltage for a voltage range of 0 to 40 Volts. In further discussions, the bias voltage has been set for each sample in order to obtain a high signal and improve the quality of the measurements.

Excitation power dependence

By contrast, the photoresponse signals from all three samples were strongly affected by the excitation power. The laser beam power has been reduced by more than 2 orders of magnitude by using attenuating filters. Instead of being a linear function of power, the photosignal was a sub-linear function of the excitation power, which suggests:

- the laser beam intensity, even attenuated by two orders of magnitude, was still too high,
- the photoconductive 'lifetimes' are strongly dependent on excitation power ('lifetimes' is under quotes because it is not accurate to talk about photoconductive lifetimes outside the weak excitation regime), which results in excitation-power-dependent responsivities,
- the presence of deep hole traps within the energy gap, because these traps would be progressively filled with increasing excitation power, resulting in the reduction in the number of holes that can recombine with the photo-generated electrons and the increase of the apparent 'lifetimes' of these electrons.

modulation frequency dependence

As in the case of the excitation power, a strong dependence of the photosignal on the modulation frequency for all three samples has been observed (Fig. VI-3). The frequency range also covered 2 orders of magnitude, from about 5Hz to 800 Hz. If the measurements had been done under equilibirum conditions, the photoresponse would have been independent of the modulation frequency. Obviously, this is not the case here as shown in Fig VI-3 and the following conclusions can be deduced:

Dependence of Photovoltage on Modulation Frequency

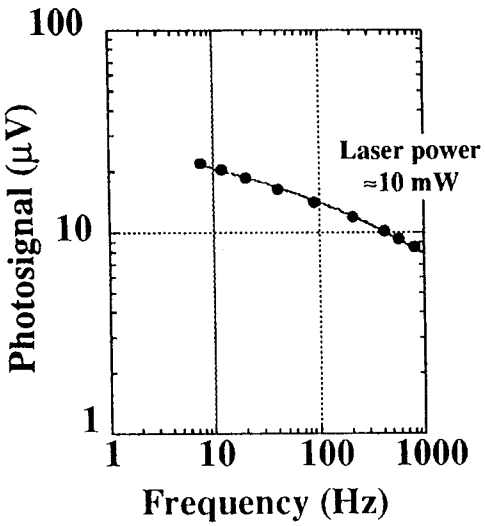

GaN #1

Thickness ≈ 1.6 μm
ρ = 0.0252 Ωcm
μ = 143 cm^2/Vs
n = 1.73E18 cm^{-3}

Bias = 20 V

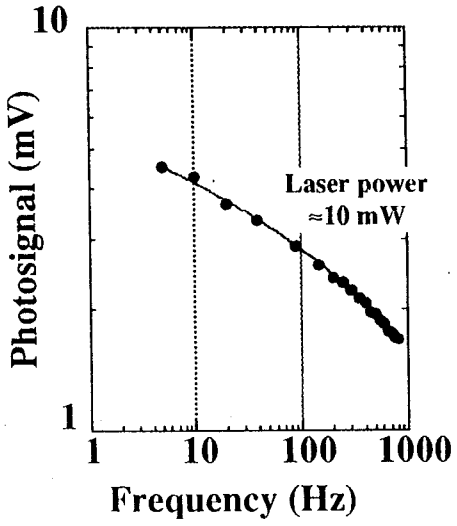

GaN #2

Thickness ≈ 1.36 μm
ρ = 0.693 Ωcm
μ = 25 cm^2/Vs
n = 3.61E17 cm^{-3}

Bias = 10 V

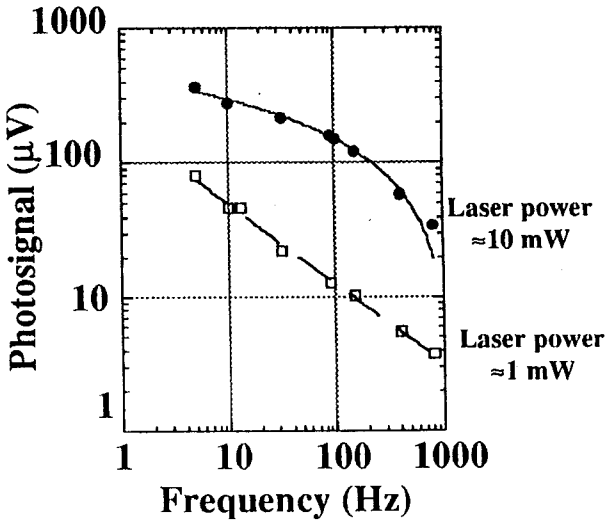

$Ga_{0.93}Al_{0.07}N$

Thickness ≈ 1.465 μm
ρ = 1.14 Ωcm
μ = 5.69 cm^2/Vs
n = 9.62E17 m^{-3}

Bias = 6 V

FIGURE VI-3

- for the level of excitation used, equilibrium conditions were not achieved,
- in view of the shapes of the spectra in Fig. VI-3, the existence of several photoconductive lifetimes, corresponding to several different recombination mechanisms, is expected.

All these preliminary measurements illustrate complicated relations between the photoconductivity signals and both the excitation power and modulation frequency. Optimum photodetectors must be operated under equilibrium conditions. Consequently, the phenomena observed here and their correlations to the physical properties of the films must be clarified. For exmaple, the relation between the hole traps and the deep levels causing the yellow photoluminescence emissions (Section III) needs to be investigated. The de-activation of these hole traps through compensation of the films will also be investigated.

Conclusion and future work

Photoconductivity lifetimes have been measured for n-type GaN and n-type $Ga_{0.93}Al_{0.07}N$ photoconductive UV detectors. The dependence of the photoresponse on the voltage bias, the excitation power and the modulation frequency has been investigated.

Further efforts are being conducted in order to obtain high quality UV photodetectors and the immediate future work will focus on:

- further measurements and correlations between the photoresponses and the physical properties of GaN and GaAlN are necessary,
- in particular, measurements on compensating films will be conducted,
- the spectral response of GaN and GaAlN detectors needs to be clearly assessed. Before the measurement apparatus is ready and reliable (see next paragraph on experimental setup), preliminary measurements will be done using gas lasers such as Ar (0.514 μm), He-Ne (0.628 μm) as well as semiconductor GaAs lasers (0.9 μm) and in-house made high-power GaInAsP laser diodes (0.808 μm),
- the measurement of the solar blindness and the identification of defects causing beyond gap responsivity,
- the development of highly doped or/and heterojunction contacts for low width devices. A better geometry for UV detector is shown in Fig. VI-3,
- the development of vertically active region devices with heterojunction contacts.

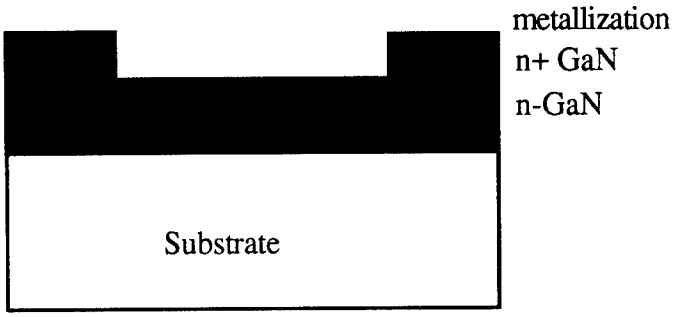

Fig. VI-3. Schematic of UV detector with heavy doped contacts.

Homemade UV-measurement setup

The CQD has purchased a high-pressure xenon lamp. This lamp is installed in parallel to the photoluminescence equipment. It uses the same monochromator, photomultiplier for signal collection and synchronous detection equipment as the PL apparatus (FIG. VI-4). Before it is used in a regular basis, this system will be calibrated. Then, UV transmission/absorption, UV reflectance, and most importantly the spectral response of $Ga_{1-x}Al_xN$ photodetectors will be possible within the CQD.

References

1- M.A. Khan, J.N. Kuznia, D.T. Olson, J.M. Van Hove, M. Blasingame, and L.F. Reitz, Applied Physics Letters 60(23), 2917 (1992).

2- M.A. Khan, J.N. Kuznia, D.T. Olson, M. Blasingame, and A.R. Bhattarai, Applied Physics Letters 63(18), 2455 (1993).

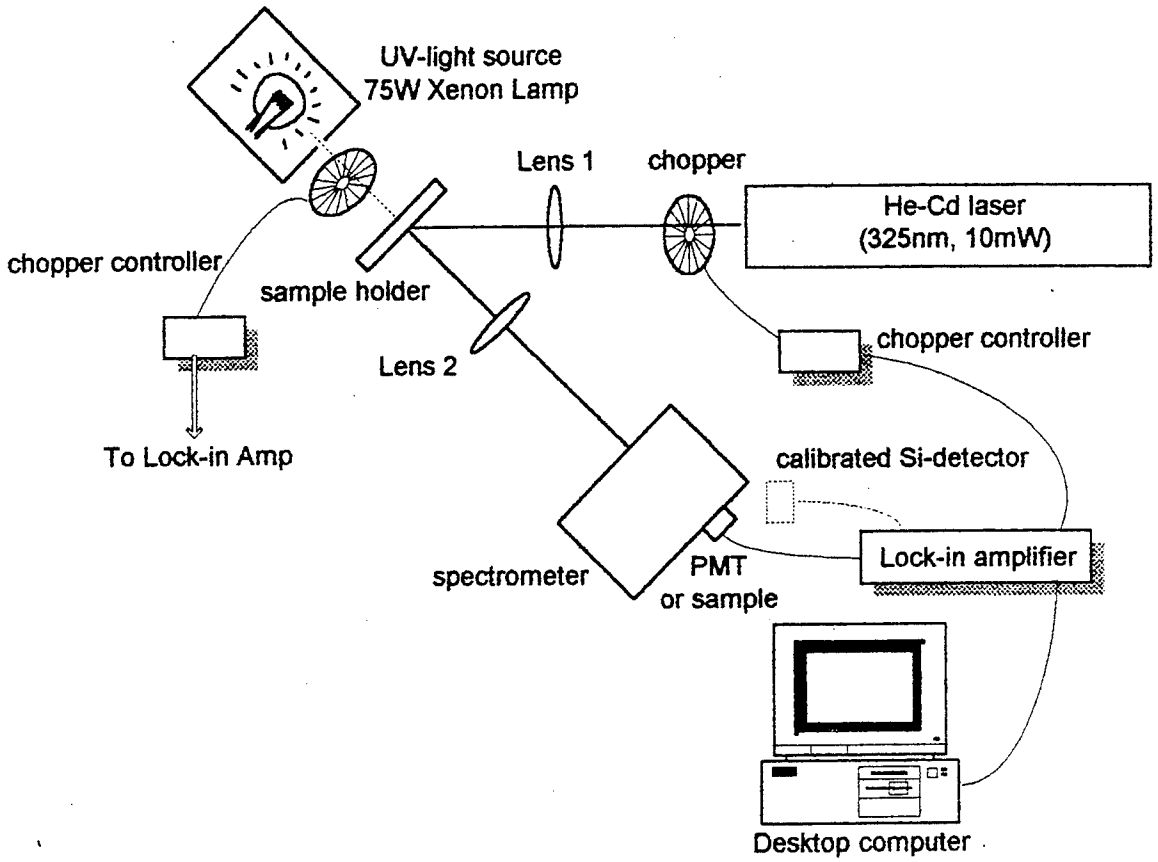

Fig. VI-4. New UV-measurement setup which is capable of: UV-PL, UV-photoresponse, UV-photoconductivity, UV reflectivity, UV transmission.

VII. MATERIAL PROCESSING

Fabrication of Contacts

Due to their large bandgaps and high dielectric constants, III-Nitrides are well suited for blue and ultraviolet optoelectronics as well as high temperature, power and frequency device applications. Blue light emitting diodes and metal-semiconductor field effect transistors (MESFETs) have already been fabricated successfully [1]. However, the immature contact technology (ohmic and rectifying contacts) for wide bandgap semiconductor GaN and AlN still constitutes an obstacle to the further advancement of III-Nitride-based electronic devices.

This is a report of the initial investigation of contacts to GaN. The first objective has been to realize ohmic contacts. Indium contacts have been used for n-type GaN, while two separate metallization schemes: Ti/Au and Au/Ge/Ni/Au (widely used in GaAs technology) have been conducted on Mg-doped GaN. Pre and post annealing surface current-voltage (I-V) measurements and surface structural strength of these contacts are presented.

Indium contact on n-type GaN

The fabrication of the indium (In) contacts entailed placing mechanically pressed and flattened In chips directly onto the surface of the GaN. The sample has then been placed in a Hall Annealer at a temperature of 650 °C, under a flow of forming gas (10% H_2 in N_2) to ensure an oxygen free environment. This helps eliminate any surface oxidation that could occur at such high temperatures. The semiconductor is then removed from the furnace and allowed to cool with the In contacts firmly attached.

Such In contact scheme has been conducted onto n-type ($n \geq 10^{17}$ cm^{-3}) GaN and showed a linear I-V relationship (Fig. VII-1). Such linear plot confirms that this contact was ohmic.

Other contacts on Mg doped GaN

Because p-type GaN has a much higher work function than n-type GaN, indium contacts are expected to exhibit a rectifying behavior when used for Mg-doped GaN. Consequently, the CQD has chosen to study contact schemes involving Au.

The fabrication of Ti/Au and Au/Ge/Ni/Au contacts was achieved by electron-beam evaporization. The contact scheme for Ti/Au utilized an initial layer of Ti about 350 Å thick capped with a layer of Au of about 2000 Å thick. The Au/Ge/Ni/Au scheme was the

n-GaN
$(00\bullet1)Al_2O_3$

Indium contacts on GaN

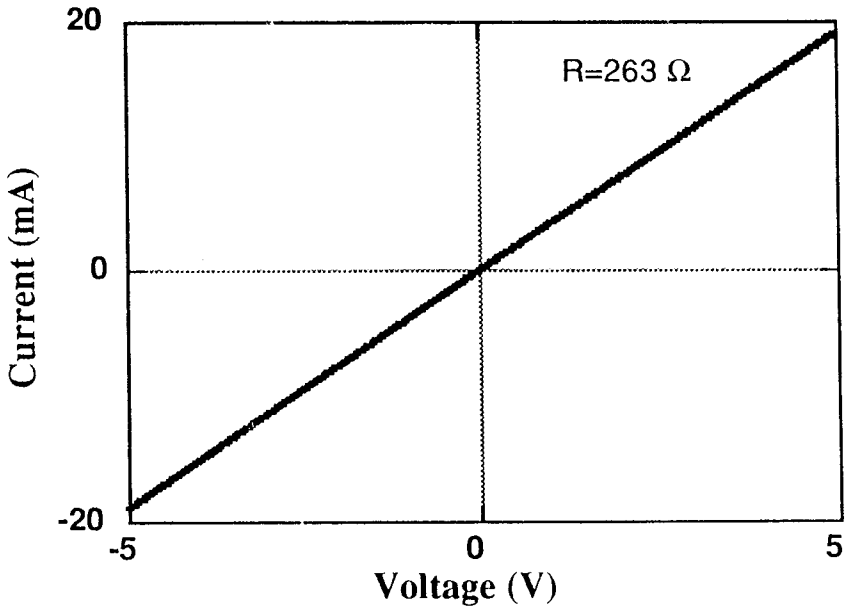

Simple indium pads pressed and melted onto the sample provide good ohmic contact to n-type GaN.

following: 700 Å of Au, 300 Å of Ge and finally 2000 Å of Ni-Au. After deposition, these contacts were patterned using standard photolithography techniques.

As deposited contacts exhibited non-linear I-V characteristics even for small currents, which shows the rectifying behavior of these contacts. Annealing experiments have then been conducted in order to improve reduce the contact resistances. Fig. VII-2 shows the non-linear I-V curve of the Ti/Au contacts on GaN before and after annealing. The barrier heights are strongly dependent on the type of contact metals. A brief annealing step of five minutes at 650 °C under forming gas reduces the barrier height in this scheme and the I-V curve reflects this change. The contact surface demonstrated the proper behavior for an annealed substance (when scratched the contact does not flake off, but rather smudges). The annealing of the Au/Ge/Ni/Au film led to an undermining of the structure of the contact. Although it passed the "scratch test", when the gold wire bonds were being applied the contacts detached themselves from the semiconductor. Therefore, the I-V characteristics could not be measured.

Interdigitated structure for photoconductors

One special structure that was investigated was Ti/Au on GaN patterned in a unique interdigital scheme. Figure VII-3 is a schematic diagram of this interdigital setup which is applied to a detector structure.

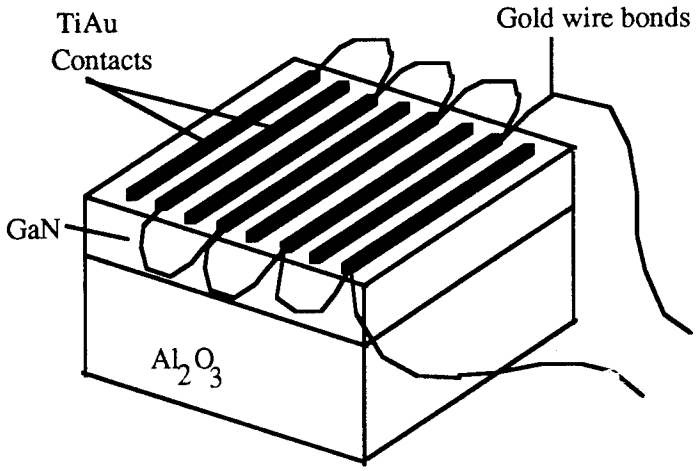

Fig. VII-3. Interdigital contact design.

The bars of Ti/Au were 50 μm wide and separated by a distance of 10 μm. Alternate bars were bonded together and hooked up to a photodetector setup. The setup is designed to give the maximum photocurrent. To date, such device structure has not been tested yet.

1.2 μm GaN:Mg
~350Å AlN
(00•1)Al_2O_3

Ti/Au contacts on GaN

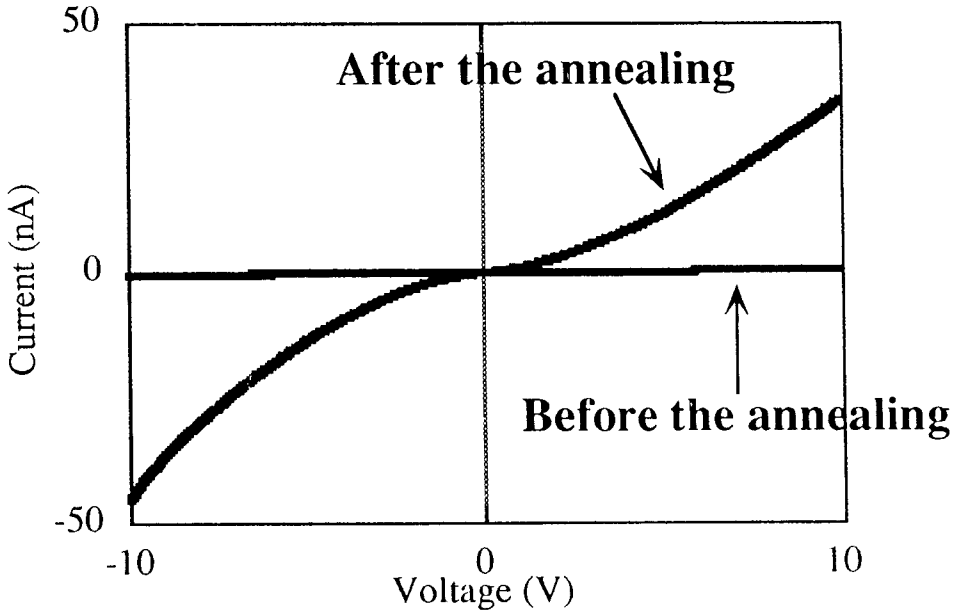

- Contacts
  - Au: 2000 Å
  - Ti: 350 Å
  - evaporated on GaN:Mg
- Annealing:
  - T anneal = 650°C
  - Time = 5 min
  - Ambient gas = forming gas
- Annealing the Ti/Au contacts reduces the contact resistance.

FIGURE VII-2

Reactive ion etching (literature review)

The realization of sub micron features in many new devices and the unavailability of a wet etch process for the III-Nitrides has established a need for a dry etching technique which is very controllable, reasonably rapid and reproducible.

Need for dry etching

Poor quality GaN films have been found to dissolve in a hot alkali solutions at a very slow rate [2]. In fact, the inherent chemical stability of these wide bandgap nitrides makes a simple and reliable wet etch process almost impossible. Moreover, the selectivity of the wet etching within the III-Nitride material system has never been investigated. Consequently, researchers have turned towards dry etching methods.

Another need for a reliable dry etching technique is heralded by the fact that most wet chemical etch processes are very isotropic and an anisotropic etch is necessary for some types of device design. In particular, it is necessary to develop dry patterning methods which are effective across the entire composition range of $In_XGa_{1-X}N$ and $In_XAl_{1-X}N$ alloys since virtually any advanced device will be based on these heterostructures [3]. Plasma processing, for these many reasons, is now seen as the only viable approach to the problem of etching III-V nitrides.

Reactive ion etching

Reactive ion etching (RIE) is a term for plasma etching that is often applied to low pressure methods (≤ 100 mTorr). The actual etching takes place through a combination of chemical and physical components. The chemical etch components are generally isotropic. This is performed when III-V material etch spontaneously upon exposure to atomic chlorine through the formation of volatile group III and group IV chlorides. Energetic ions also strike the surface of the semiconductor sample, leading to sputtering of its surface. This anisotropic event is the purely physical component of the etching. The speeds at which these two mechanisms occur at are also different: the chemical etching is rapid while the physical etching is slow. In all dry etching techniques, the chemical and physical components are traded off to achieve the desired result.

Reactive ion etching is typically performed in the 10 to 100 mTorr pressure range in a parallel plate or diode-type reactor [3,4,5]. Radio frequency (RF) power, usually 13.56 MHz, is applied through a coupling capacitor to ignite and sustain the discharge. The more massive ions in the discharge are unaffected by the RF applications, yet the electrons respond to it. This causes the reactor wall to charge negatively with respect to the body of

the plasma. The result of this charge build up is a space charge region produced along the reactor walls. Ions which stray near this region are accelerated across it [4]. If the electrodes are not equal in size then there will be a stronger field concentrated on the smaller electrode. Any sample placed on this electrode (powdered) will be bombarded by ions, neutral gas atoms and molecules from the plasma. The electrons are 'heated' by the applied field to ~10 eV while the neutral and ion temperature is usually ~1 eV [4].

RIE is by far the most popular dry etching technique used for III-V materials because it takes advantage of the physical as well as chemical etching mechanisms [2,3,4]. In fact, the etch rates for RIE are faster than the sum of the physical and chemical components due to the fact that the volatile etch products formed by chemisorption are quickly removed from the surface of the material by physical sputtering, exposing a fresh layer of the material. In more details, the etching gas is chosen so as to produce species which will react chemically with the material to be etched to form a reaction product which is volatile (preferably at room temperature). The etch product then spontaneously desorbs from the surface of the etched material into the gas phase, where it is removed by the vacuum pumping system [6].

Hybrid ECR-RF technique

A particularly useful and versatile approach is the hybrid electron cyclotron resonance (ECR)-RF reactor [7]. Microwave oscillations (2.45 GHz) in a cavity creates a plasma within a quartz vacuum containment vessel. The electrons in the plasma travel along helical paths due to magnets around the quartz vessel. The magnetic field strength ($B=8.75 \times 10^{-2}$ T) creates a processional frequency (2.45 GHz) which is resonant with the applied microwave power [4]. This causes the degree of ionization in the ECR zones to be much higher than with conventional RF discharges (about 10% compared to 0.1-1% for RF). As with RIE, the active species from the plasma diffuse to the sample position, which is separately biased by an RF power application to control the bombardment of ion energy [4]. A schematic view of the ECR source is shown in Fig. VII-4.

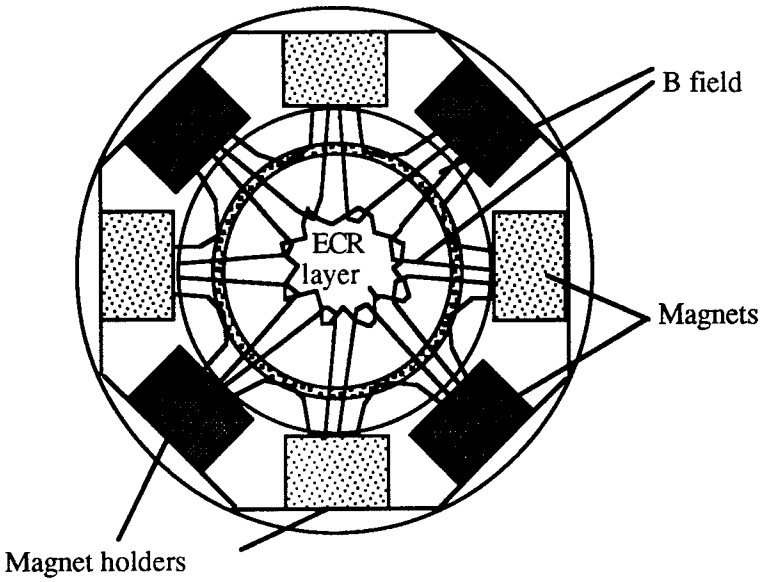

Fig. VII-4. An ERC source schematic.

The major advantage of the hybrid ECR-RF system is that a faster etch than with RF is possible due to the enhanced discharge. This means that lower ion energies can be utilized while still retaining practical etch rates. At the low pressures used (1 mTorr), the etching is also extremely isotropic. A subsequent advantage of using lower ion energies is that this leads to lower levels of damage in the semiconductor.

Ion Damage

When the semiconductor surface is struck by energetic ions, displacement damage consisting of point defects are caused in the material. Some of these defects result in deep levels within the forbidden gap [4]. These levels trap charge carriers and therefore reduce the current density in the region near the dry-etched surface. These deep levels are also usually non-radiative, therefore the optical properties of the semiconductor are significantly affected [4]. Changes to the electrical and optical properties of the semiconductor are minimized by using the hybrid ECR-RF approach. The roughness found on surfaces of samples is also reduced when using ECR or other enhanced plasma sources due to the lower DC biases employed [8].

Plasma Chemistries

The dry etching of III-V materials traditionally involves chlorine-based plasmas [3,4,7]. Additions of argon, helium, or oxygen provide easier ignition of the plasma, more stable operation or dilution to control the etch rate. Typical gases employed include Cl_2,

$SiCl_4$, BCl_3 or CCl_2F_2. Dry etching often changes the stoichiometry of the near-surface region of the semiconductor, and plasma related residues are usually present. These residues are generally removed by wet chemical cleaning [4]. Bromine-based discharges will also etch III-V semiconductors. At the low pressures, the etching is relatively slow, but the morphologies are smooth [3]. Iodine-based chemistries are particularly effective for etching indium-based III-V materials because the volatility of InI_3 is much greater than the chloride or bromide counterparts.

Conclusion

It has been made clear that dry etching offers many advantages over wet etching for device fabrication. These advantages include a better dimensional control, superior uniformity, compatibility with multichamber processing and less effluents. However, the disadvantages include the much higher capital equipment and to a lesser degree the question of ion damage to the semiconductor.

This review shows the still immature etching technology applied to III-Nitrides. However, in view of this review, the CQD will soon acquire the most appropriate RIE appratus in order to process its samples to realize optimized photodetector structures in the GaAlN material system.

References

1. M.E. Lin, F.Y. Huang, and H. Morkoç, Applied Physics Letters 64, 2557 (1994).
2. M.E.Lin, Z.F. Fan, L.H. Allen, and H. Morkoç, Applied Physics Letters 64, 887 (1994).
3. S.J.Pearton and C.R. Abernathy, Applied Physics Letters 64, 3643 (1994).
4. S.J. Pearton and F. Ren, J. Mat. Sci.: Mat. In Elec. 5, 1 (1994).
5. S.J. Pearton, C.R. Abernathy, F. Ren, J.R. Lothian, P.W. Wisk, A. Katz and C. Constantine, Sem. Sci. and Tech. 8, 310 (1992).
6 J.W. Coburn, Plasma etching and Reactive ion etching, American Institute of Physics, New York, NY (1982).
7. S.J. Pearton, C.R. Abernathy, F. Ren, J.R. Lothian, P.W. Wisk and A. Katz, J.Vac. Sci. Technol. A 11, 1772 (1993).
8. S.J. Pearton and C.R. Abernathy, Applied Physics Letters 64, 2294 (1994).

VIII. FUTURE WORK

Undoped binary componuds

The future of the research work on undoped binary III-Nitride compounds will be to investigate the correlation between the structural and optical quality of GaN, and to interpret the origin of the deep-level associated yellow luminescence observed from GaN.

Mg and Ge doped GaN

The future work in this area will be to achieve the p-type doping control of GaN. Since the preliminary results presented here show that too little amount of Mg has been incorporated, this amount will be increased. The possibility to achieve p-type doping without any post-growth treatment will be investigated. The n-type doping control of GaN will be improved by using SiH_4 as well as GeH_4.

Ternary compounds GaAlN

Following the growth and the n-type doping of high quality $Ga_{1-x}Al_xN$, the CQD will start the p-type doping of these alloys with Mg. Heterostructures with GaN and AlN will be realized to achieve p-n and p-i-n junction UV photodetectors.

Material processing

The current work on the realization of ohmic contacts will be pursued, in particular for contacts on Mg-doped GaN. The dry etching of high quality GaN and AlN will be investigated as soon as an appropriate dry etching system is available.

UV Photodetectors

Further measurements will be conducted on GaN and GaAlN photoconductors in order to determine the correlations between the photoresponses and the physical properties of III-Nitride materials. The spectral response and most importantly the solar blindness of these detectors will be assessed. The realization of highly doped or/and heterojunction contacts, as well as the realization of better detector geometries will be investigated.

IX. APPENDIX

List of publications and invited talks between 7/1/94-3/31/95 (contract No. N00014-93-1-0235)

1- "*Photoluminescence study of GaN ondifferent substrates*
X. Zhang, P. Kung, A. Saxler, and M. Razeghi,
In preparation.

2- "*Future Semiconductor Materials for Optoelectronics*"
M. Razeghi,
Heterostructures in Science and Technology, Würzburg, Germany, March 13-17,1995.

3- "*High quality AlN and GaN epilayers grown on (00•1) sapphire, (100) and (111) silicon substrates*"
P. Kung, A. Saxler, X. Zhang, D. Walker, T.C. Wang, I. Ferguson, and M. Razeghi,
Applied Physics Letters 66(22), (May 29th 1995).

4- "*Low pressure metalorganic chemical vapor deposition of high quality AlN and GaN thin films on sapphire and silicon substrates*"
P. Kung, X. Zhang, E. Bigan, and M. Razeghi; A. Saxler,
Presented at SPIE Photonics West'95, San Jose, CA, February 6-9, 1995.

5- "*Second harmonic generation in hexagonal SiC*"
P. Lundquist, W.P. Lin, and G.K. Wong; M. Razeghi; J.B. Ketterson,
To be published in Applied Physics Letters, (1995).

6- "*Epitaxial Growth of Aluminum Nitride on Sapphire and Silicon*"
K. Dovidenko, S. Oktyabrsky, J. Narayan, and M. Razeghi,
MRS 1994 Fall Meeting, Boston, MA, November 28-December 2, 1994.

7- "*High Quality Mg-Doped AlGaN Thin Films Grown on Basal Plane Sapphire Substrate*"
C.J. Sun, P. Kung, A. Saxler, T.C. Wang, and M. Razeghi,

MRS 1994 Fall Meeting, Boston, MA, November 28-December 2, 1994.

8- *"LP-MOCVD Growth of High Quality GaN and AlN Thin Films"*
A. Saxler, P. Kung, X. Zhang, and M. Razeghi; H. Jürgensen,
Presented at the Wide Bandgap Nitrides Workshop, St Louis, MO, October, 1994.

9- *"Photoluminescence of GaN grown on silicon substrates"*
P. Kung, A. Saxler, C.J. Sun, T.C. Wang, and M. Razeghi,
CAM 94 Physics Meeting, Cancún, Mexico, September 26-29, 1994.

10- *"MOCVD growth and characterization of III-Nitride for optoelectronic device applications"*
Ph.D. dissertation of Chien-Jen Sun, Ph.D. Final exam 9/29/94, Degree awarded date June 1995.

REPORT DOCUMENTATION PAGE

Form Approved
OMB No. 0704-0188

1. AGENCY USE ONLY (Leave blank)	2. REPORT DATE	3. REPORT TYPE AND DATES COVERED
	April 1995	Annual Technical, 7/1/94-3/31/95

4. TITLE AND SUBTITLE
Metalorganic Chemical Vapor Deposition of GaN, AlN and GaAlN for UV Photodetector Applications

5. FUNDING NUMBERS

6. AUTHOR(S)

Manijeh Razeghi

7. PERFORMING ORGANIZATION NAME(S) AND ADDRESS(ES)

Office of Naval Research
Electronics Division, Code 314
800 N. Quincy Street
Arlington, VA 22217-5660

8. PERFORMING ORGANIZATION REPORT NUMBER

9. SPONSORING/MONITORING AGENCY NAME(S) AND ADDRESS(ES)

10. SPONSORING/MONITORING AGENCY REPORT NUMBER

11. SUPPLEMENTARY NOTES

12a. DISTRIBUTION/AVAILABILITY STATEMENT

Approved for Public Release: Distribution Unlimited

12b. DISTRIBUTION CODE

13. ABSTRACT *(Maximum 200 words)*

GaN, AlN and GaAlN epilayers were grown by low-pressure metalorganic chemical vapor deposition, on sapphire, silicon, and 6H-SiC. The X-ray diffraction linewidths were as low as 30 and 100 arcsecs for GaN and AlN respectively on sapphire. Sharp optical absorption edges were obtained for these films. Transmission electron microscopy characterized the films microstructurally. Photoluminescence (PL) at 300 and 77 K yielded linewidths of about 80 and 40 meV respectively for GaN on all substrates. However, no deep-level-associated yellow emission was detected from the GaN on SiC. Unintentionally n-type doped GaN had an electron mobility as high as 200 cm^2/Vs at 300 K. As-grown semi-insulating GaN was also achieved. Ge doped GaN n-type (n up to 10^{20} cm^{-3}). P-type doping was conducted with Mg, resulting in semi-insulating layers. No yellow emission was detected from doped films. Ternary $Ga_{1-x}Al_xN$ was grown for $0 \le x \le 1$, with sharp and tailored absorption edges. Simple photoconductors were realized with GaN and $Ga_{1-x}Al_xN$. The lifetimes of the excess carriers were investigated. The processing of GaN and GaAlN films (deposition, annealing of contacts) was conducted.

14. SUBJECT TERMS	15. NUMBER OF PAGES
MOCVD, GaN, AlN, GaAlN, sapphire,silicon, SiC, X-ray diffraction TEM, optical absorption, photoluminescence, deep-level yellow emission, Ge, n-type, Mg, photoconductors, contacts	48
	16. PRICE CODE

17. SECURITY CLASSIFICATION OF REPORT	18. SECURITY CLASSIFICATION OF THIS PAGE	19. SECURITY CLASSIFICATION OF ABSTRACT	20. LIMITATION OF ABSTRACT
Unclassified	Unclassified	Unclassified	